Modeling and Finite Element Simulations of Ceramic Paste Extrusion in 3D Printing

by

Kuralay Baiseitova

Submitted to the Department of Mathematics
in partial fulfillment of the requirements for the degree of

Master of Science in Applied Mathematics

at the

NAZARBAYEV UNIVERSITY

July 2020

Author .....
Department of Mathematics
July 30, 2020

Certified by .....
Dr. Piotr Skrzypacz
Assistant Professor
Thesis Supervisor

Accepted by .....
Daniel Pugh
Dean, School of Science and Humanities

Modeling and Finite Element Simulations of Ceramic Paste Extrusion in 3D Printing

by

Kuralay Baiseitova

Submitted to the Department of Mathematics
on July 30, 2020, in partial fulfillment of the
requirements for the degree of
Master of Science in Applied Mathematics

Abstract

Ceramic paste extrusion process, such as 3D printing, is commonly used for fabricating high quality products, like catalyst pellets for heterogeneous catalytic reactors, porous catalyst for cleaning gas released from an auto, ceramic block packing for immediate heat conduction adsorption process. Ceramic pastes can be characterized as non-Newtonian fluid. The extrusion of ceramic paste is complicated procedure which is controlled by viscosity of the paste, form of the extruder and die, and other operation restrictions. Meaningful part in performing the extrusion process to produce high quality extrudates of requested shape, structure and resistance are modeling and numerical analysis of extrusion process. The mathematical model is based on continuity and momentum equations which describe the motion of non-Newtonian fluid characterized by the modified Herschel-Bulkley model. Numerical simulations of ram extrusion process are provided in this work. Finite Element Method implemented in the COMSOL Multiphysics software is used to simulate the paste flow in the ram extruder. Numerical study shows that the die geometry and paste velocity significantly affect the distribution of pressure. The outcomes of simulations in COMSOL Myltiphysics software are presented in 1D, 2D and 3D plots. The velocity of ceramic paste reaches its maximum value at the centre of the extrusion die and decreases towards the die walls. Moreover, the viscosity of alumina paste in transition region was computed numerically. The shear rate of the paste steadily decreases in the extrusion die. As a result, the pressure of the fluid inside of extrusion die is constant and of high magnitude in the barrel and it slowly decreases as the fluid moves to the die outlet with a small diameter.

Thesis Supervisor: Dr. Piotr Skrzypacz
Title: Assistant Professor

Acknowledgements

Firstly, I would like to thank my thesis supervisor Professor Piotr Sebastian Skrzypacz for his guidance, help and extensive support throughout my research work. Professor Skrzypacz shared his valuable experience and taught me how to perform numerical simulations using COMSOL Multyphysics software. I am also gratefull to Professor Boris Golman for helping me better understanding the extrusion process from engineering point of view.

I would like to acknowledge members of my Thesis Committee, Professor Anastasios Bountis and Professor Friedhelm Schieweck, for their comments and suggestions needed for improvement of my thesis.

Finally, I would like to thank my family, my class mates and friends for their moral support and motivation during this process.

Contents

Chapter 1

Introduction

Extrusion of ceramic pastes is complicated process that depends on rheological properties of paste, geometry of the extruder and die. Those properties are determined by the volume, distribution and size of fraction particles, characteristic of the surface and load and features of binder [2]. The processing and transport characteristics of slurries in the ceramic industry are strongly dependent on their rheological properties [1]. Understanding of the rheological parameters is highly essential, especially when transporting of a large amount of paste. A simplified scheme of 3D printing device is illustrated in Fig. 1-1. Moreover measuring flow and viscosity curves, the

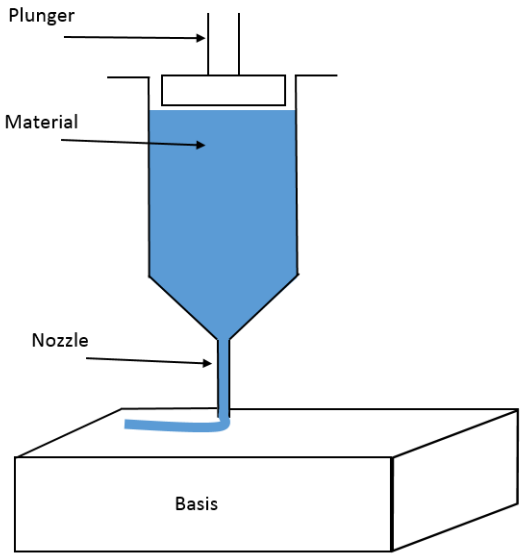

Figure 1-1: 3D printing device.

yield point can be computed as well, e.g. by using the Herschel-Bulkley model. Estimating the viscosity function and the yield point provides an important information for better understanding of behaviour of paste flow in extruders. It is also helpful for solving problems with slurry which is difficult to pump [3]. The extrusion process for ceramic paste has been also studied in [1] where authors used the same modified Herschel-Bulkley model. They have studied the influence and behaviour of the air bubble that is trapped in the extrusion die during the preparation and loading of the paste [1].

Meaningful part in performing the extrusion to produce high quality extrudates of requested shape, structure and resistance are modeling and numerical analysis of the mathematical extrusion model. In this work, the equation of the motion of incompressible fluids whose viscosity depends nonlinearly on pressure and shear rate will be discretized by Finite Element Method. There exists a wide class of fluids, namely non-Newtonian fluids, whose properties can not be circumscribed by standard Navier-Stokes equations. Fluids with shear rate and pressure-dependent viscosity are essential part of non-Newtonian fluids. There are numerous applications where this type of fluids can play a an important role, e.g., 3D printing, blood rheology, geology and chemical engineering [4, 5]. Fluids with pressure-dependent viscosity appear in various industrial applications, for instance where the high pressure occurs. This work shows that applied computational modelling is a useful tool to design and optimize complicated ceramic extrusion for 3D printing.

Chapter 2

Herschel-Bulkley model

Extrusion process of ceramic pastes in 3D printing is complex approach which is based on rheological properties of the fluid. Interpretation of parameters of the viscous fluid is highly essential, especially in field of industry. Fluids with different types of viscosity, i.e. Newtonian fluid and non-Newtonian fluid, will be considered in this chapter. Models and flow curves for Bingham plastic and regularization, that we are going to use for modeling of ceramic paste extrusion are also described further.

2.1 Newtonian fluid

Newtonian fluid is a fluid whose viscosity does not change with time, type or rate of deformation. In other words, the fluid is called Newtonian if tensors characterising the strain rate and the viscous stress are associated by constant velocity tensor which is not dependent on velocity $\boldsymbol{v}$ of the flow and stress state.

Sir Issac Newton first defined behavior of fluids by using linear relation of shear rate and shear stress which is also well-known as Newton's Law of viscosity, where constant μ describes the dynamic viscosity of the fluid as

$$\boldsymbol{\tau} = \mu\dot{\boldsymbol{\gamma}}$$

Here, $\boldsymbol{\tau}$ is the viscous stress tensor and $\dot{\boldsymbol{\gamma}} = \nabla\boldsymbol{v} + (\nabla\boldsymbol{v})^T$ stands for the rate-of-strain

tensor. Examples of Newtonian fluid are air, water, alcohol, gasoline. The Newtonian equation shows the behaviour of the flow of an ideal liquid. Dynamic viscosity, which is also called as apparent viscosity, characterises fluid's resistance of deformation. It is the ratio of the shear stress magnitude to the shear rate magnitude

$$\mu = \frac{\tau}{\dot{\gamma}}\,.$$

The magnitudes of stress and rate-of-strain tensors are respectively defined as follows [23]

$$\tau = \sqrt{\frac{1}{2}\boldsymbol{\tau} : \boldsymbol{\tau}} \quad \text{and} \quad \dot{\gamma} = \sqrt{\frac{1}{2}\dot{\boldsymbol{\gamma}} : \dot{\boldsymbol{\gamma}}}\,,$$

where : stands for the inner product of tensors. In the case of Newtonian fluid, the dynamic viscosity provide a constant value μ which means a linear relationship between τ and $\dot{\gamma}$.

2.2 Non-Newtonian fluid

On the contrary to Newtonian fluids, non-Newtonian fluids are characterized by the non-linear dependence between shear rate and shear stress or have initial yield stress or time-dependent viscosity. This is due to the complex structure and effects of deformation exhibited by the fluid materials. There are various types of non-Newtonian fluids. They can be described as pseudoplastic, viscoplastic and dilatant fluids. The graph presented below illustrates viscosity of Newtonian, shear thinning and shear thickening fluids.

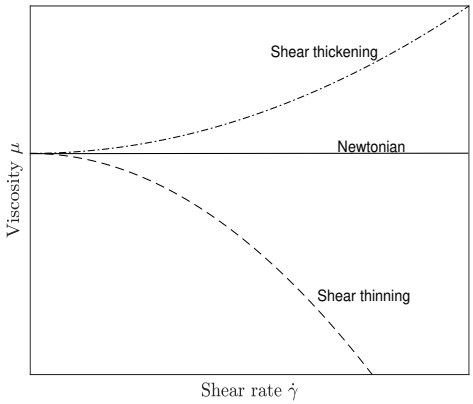

Figure 2-1: The viscosity of Newtonian and non-Newtonian fluids.

2.2.1 Pseudoplastic Fluids

Shear thinning (pseudoplastic, $\frac{\partial \mu}{\partial \dot{\gamma}} < 0$) behaviour of fluid is observed if viscosity inversely depends on shear rate. Pseudoplastic fluids become thinner while the shear rate is increasing, till the viscosity of the fluid achieves the limit of viscosity [6]. This behaviour is because of increasing the shear rate and the units suspended in the fluid will move to the same direction of the current. There will be a deformation of the fluid structure implying a breaking of aggregates at some shear rate and this will be the reason of limit viscosity. For pseudoplastic fluid material the viscosity is not affected by the time that shear rate is applied and these material don't have memory property i.e. if the force is applied and the structure is affected once, the material will not restore that structure [6]. Those fluids are also known as pseudo-plastic which is widespread in industrial and biological systems. Examples of shear thinning are ketchup, blood, whipped cream and nail polish.

2.2.2 Viscoplastic fluids

Viscoplastic fluids behave similar to pseudoplastic fluids upon yield stress. They need precalculated shear stress in order to start moving. Common example of these, the Bingham plastic, that needs the shear rate to exceed a minimal yield stress value instead of going from high viscosity to low [6]. After this changing a linear relationship

between the shear rate and shear stress will take over. Examples of viscoplastic fluids can be blood, ketchup and some sewage sludge's.

2.2.3 Dilatant fluids

A fluid whose viscosity directly proportional to the shear rate is shear thickening which is also called dilatant ($\frac{\partial \mu}{\partial \dot{\gamma}} > 0$). Similar to the pseudoplastic fluids the stress period hasn't influence, i.e. if material is broken or the structure destroyed it will not go backwards to its previous state [6]. Common examples of dilatant fluids are honey, cement and ceramic mixture. Combination of cornstarch and water is typical example of shear thickening behaviour of the fluid. If you squeeze this mixture it feels like solid since molecules of fluid line up. Also cornstarch suspension act as a liquid when no one applying the pressure on the surface because the molecules are relaxed at that time.

In classical fluid mechanics, the Cauchy stress tensor $\boldsymbol{\tau}$ depends on the velocity gradient $\nabla \boldsymbol{v}$ and the density ρ. Here, $\boldsymbol{v} = (v_1, \ldots, v_n)$ denotes the velocity field. By the principle of material frame-indifference we can say that the stress tensor $\boldsymbol{\tau} = \boldsymbol{\tau}(\dot{\boldsymbol{\gamma}})$ depends on symmetric part of the velocity gradient $\dot{\boldsymbol{\gamma}} = 2\,\boldsymbol{D}\boldsymbol{v} \in R^{n\times n}_{sym}$ [10]

$$\boldsymbol{D}\boldsymbol{v} = \frac{1}{2}(\nabla \boldsymbol{v} + \nabla \boldsymbol{v}^T) \quad \text{where} \quad (\boldsymbol{D}\boldsymbol{v})_{i,j} = \frac{1}{2}\left(\frac{\partial v_i}{\partial x_j} + \frac{\partial v_j}{\partial x_i}\right).$$

The following constitutive equation shows the relation between the stress tensor $\boldsymbol{\tau}$ and the rate-of-strain tensor [9]

$$\boldsymbol{\tau}(\dot{\boldsymbol{\gamma}}) = -p\boldsymbol{I} + \mu(\dot{\gamma})\dot{\boldsymbol{\gamma}}\,. \tag{2.1}$$

In the particular case of $\mu = \text{const}$ the fluid is included to the class of Newtonian fluids. In all other cases the fluid is considered as a non-Newtonian fluid. A significant part of non-Newtonian fluids can be determined according to the relation $\mu = \mu(\dot{\gamma})$. Examples of non-Newtonian models with shear dependent viscosity are listed below [11].

Ostwald-de Waele power law [12, 13]

$$\mu(\dot{\gamma}) = \mu_0 \, \dot{\gamma}^{n-2}$$

Examples: molten chocolate, aqueous dispersion of polymer latex spheres, starch, clay suspensions

Carreau Carreau-Yasuda [14, 15]

$$\mu(\dot{\gamma}) = \mu_\infty + \frac{\mu_0 + \mu_\infty}{(1 + \alpha \dot{\gamma}^\alpha)^{\frac{n}{2}}}$$

$$\mu(\dot{\gamma}) = \mu_\infty + (\mu_0 - \mu_\infty)(1 + \alpha \, \dot{\gamma}^\alpha)^{\frac{n-1}{\alpha}}$$

Examples: molten polystyrene, polyacrylamide [11].

Cross [16]

$$\mu(\dot{\gamma}) = \mu_\infty + \frac{\mu_0 - \mu_\infty}{1 + \alpha \, \dot{\gamma}^n}$$

Examples: aqueous polyvinyl acetate dispersion, aqueous limestone suspension [11].

Eyring [17, 18]

$$\mu(\dot{\gamma}) = \mu_\infty + (\mu_0 - \mu_\infty) \frac{\operatorname{arcsinh}(\alpha \, \dot{\gamma})}{\alpha \, \dot{\gamma}}$$

Examples: napalm (co precipitated aluminum salts of naphthenic and palmitic acids, jellied gasoline), 1% nitrocelulose in 99% butyl acetate [11].

Sisko [19]

$$\mu(\dot{\gamma}) = \mu_\infty + \alpha \, \dot{\gamma}^{n-1}$$

Examples: lubricating greases [11].

By analysing the flow index n we can specify the behaviour of the fluid. As the index n approaches to 1, the behaviour of the fluid is going to pass from shear thinning to shear thickening fluid [6]. In case if $n > 1$, the fluid has shear thickening behaviour. According to Seyssiecq and Ferasse [7] the fluid behaviour can be described

as follows [6]

$$\tau_0 = 0, \quad n = 1 \rightarrow Newtonian\ behaviour$$

$$\tau_0 = 0, \quad n < 1 \rightarrow Pseudoplastic\ behaviour$$

$$\tau_0 > 0, \quad n = 1 \rightarrow Bingham\ plastic\ behaviour$$

$$\tau_0 = 0, \quad n > 1 \rightarrow Dilatant\ behaviour$$

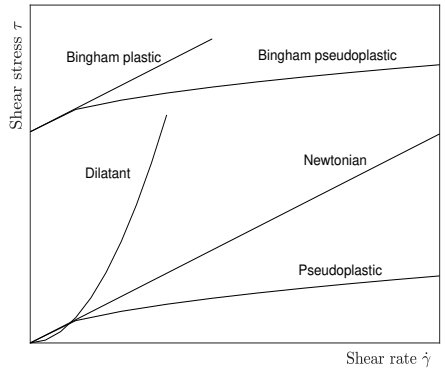

Figure 2-2: Classification of non-Newtonian fluids

2.3 Bingham model

Bingham plastic is a fluid that at low stresses acts as solid body but flows as a viscous material at the high stress rate. The Bingham model describes the flow curve of material with yield stress and constant viscosity at stresses above the yield (as pseudo-Newtonian fluid). As a typical example of Bingham plastic we mention a toothpaste. The yield stress τ can be defined as the initial force that must be applied to in order to start moving. It represents the resistance of the fluid structure to deformation or destruction. The yield stress is extremely important to consider the case when mixing reactor materials, since the yield stress is affecting the physico-chemical characteristics of the fluid. One should apply some pressure to the tube so that the paste will extrude.

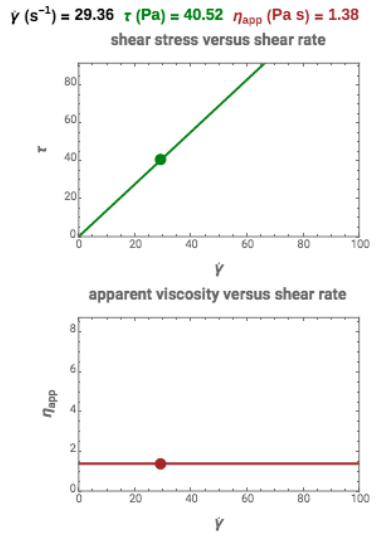

(a) Newtonian fluid: $\tau_0 = 0$ and $n = 1$.

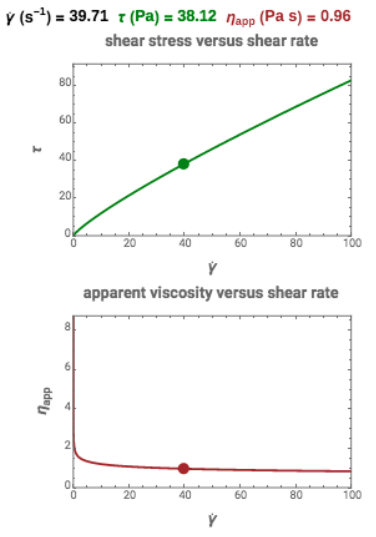

(b) Pseudoplastic fluid: $\tau_0 = 1$ and $n < 1$.

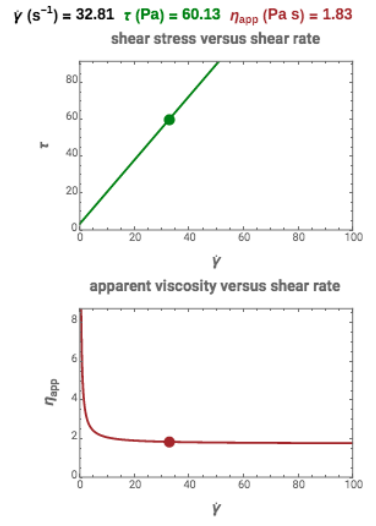

(c) Bingham fluid: $\tau_0 > 1$ and $n = 1$.

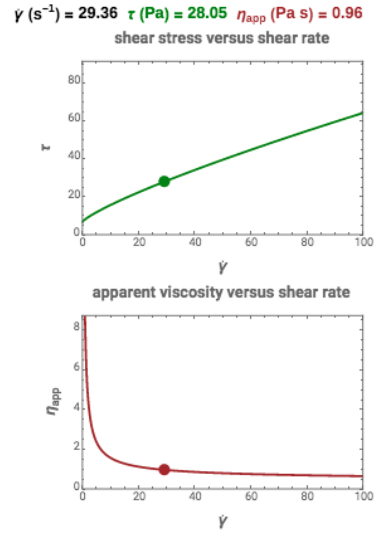

(d) Bingham fluid: $\tau_0 > 1$ and $n < 1$.

Figure 2-3: Graphs of flow curves of Herschel-Bulkey model represent the dependencies of shear stress vs shear rate and viscosity vs shear rate for different values of yield stress, shear rate and flow index [22].

Herschel and Bulkley [20] proposed the following model

$$\begin{aligned} \mu(\dot{\gamma}) = k\,\dot{\gamma}^{n-1} + \frac{\tau_0}{\dot{\gamma}} \quad &\text{if} \quad \tau \geq \tau_0 \\ \dot{\gamma} = 0 \quad &\text{if} \quad \tau < \tau_0 \end{aligned} \tag{2.2}$$

where $\mu(\dot{\gamma})$ stands for the nonlinear viscosity, $\dot{\gamma}$ represents the shear rate of the fluid,

k is the consistency factor and n is the Herschel-Bulkley fluid index (in our case n is chosen as $0 < n < 1$ for shear-thinning) which also controls the fluid behavior [20]. The apparent viscosity is $\eta = \mu = \frac{\tau}{\dot{\gamma}}$. According to numerical values of the shear stress and viscosity at the fixed parameter of the shear rate Fig. 2-3 shows the graphs of τ versus $\dot{\gamma}$ and μ versus $\dot{\gamma}$ for Herschel-Bulkley model $\tau = k|\dot{\gamma}| + \tau_0$. These plots that demonstrate the dependency of shear rate and shear stress have been prepared in [22] using online Wolfram Demonstration Project. The yield stress τ_0 is equal to shear stress τ if shear rate $\dot{\gamma}$ is zero and the viscosity μ of the fluid is the slope of the curve at stresses above the yield stress. For the Bingham plastic model shear stress τ is described as [21]

$$\tau = \tau_0 + \mu\dot{\gamma}^n$$

where τ_0 is the yield stress. If $\tau_0 = 0$, then the fluid has Newtonian behaviour. If $\tau_0 > 1$, then it has Bingham model behaviour. The equivalent relationship for Casson fluid in case when $\dot{\gamma} > 0$

$$\sqrt{\tau} = \sqrt{\tau_0} + \sqrt{k_c\dot{\gamma}}$$

where k_c is viscosity parameter. Let us transform this equation into

$$\tau = \tau_0 + [k_c + 2\sqrt{\tau_0 k_c}\dot{\gamma}^{-1/2}]\dot{\gamma}$$

For the *Herschel-Bulkley fluid* our model gets the following form

$$\tau = \tau_0 + k_H\dot{\gamma}^{n-1}\dot{\gamma}$$

where k_H denotes the viscosity parameter. The Herschel-Bulkley model is characterized by the non-linear behavior and yield stress. The consistency parameter k_H describes the fluid viscosity. In order to be able to analyze k_H consistency index parameters for various of fluids, they should have similar behaviour of the flow index n. All above models are illustrated in figure below

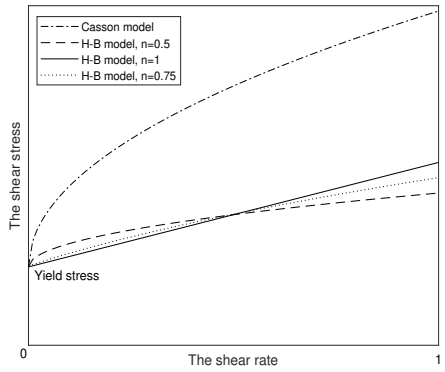

Figure 2-4: Shear stress vs. shear rate in various constitutive models.

2.3.1 Regularization of viscosity

It is a well known fact that that the viscosity of the fluid depends on the deformation process for non-Newtonian fluid. The Herschel-Bulkley model can be considered as one of the most common definition of non-Newtonian fluids, as an example of fluid with yield stress and nonlinear dependency of stress-strain in yielded region. It can be counted as a mix of Bingham plastic and power law fluids [20]. The general model is described as

$$\mu(\dot{\gamma}) = k\dot{\gamma}^{n-1} + \frac{\tau_0}{\dot{\gamma}} \quad \text{if} \quad \tau \geq \tau_0\,,$$
$$\dot{\gamma} = 0 \quad \text{if} \quad \tau < \tau_0\,.$$

Bingham plastics are a particular example of Herschel-Bulkley fluids in the same way as Newtonian fluids with viscosity model of power-law type.

The general form of Herschel-Bulkley model does not consider the problem for unyielded region ($\dot{\gamma} > 0$). This type of regularization was done by Tanner and Milthorpe [32], who modified the original Bingham model by using *bi-viscosity model*, where there are two slopes of finite viscosity, namely the viscosity μ_0 for $\dot{\gamma} < \dot{\gamma}_c$ and viscosity $\mu \ll \mu_0$ for $\dot{\gamma} > \dot{\gamma}_c$ [24]. In the case of $\dot{\gamma} < \frac{\tau_0}{\mu_0}$ solid substance behaves as extremely viscous fluid whose viscosity is μ_0 [33]. When strain rate passes the yield

stress threshold τ_0, the fluid behaves according to the power-law

$$\mu(\dot{\gamma}) = \begin{cases} \frac{\tau_0}{\dot{\gamma}} + k\left(\frac{\dot{\gamma}}{\dot{\gamma}_c}\right)^{n-1} & \text{for} \quad \dot{\gamma} \geq \dot{\gamma}_c\,, \\ \tau_0 \frac{(2-\dot{\gamma}/\dot{\gamma}_c)}{\dot{\gamma}_c} + k\left[(2-n) + (n-1)\frac{\dot{\gamma}}{\dot{\gamma}_c}\right] & \text{for} \quad \dot{\gamma} < \dot{\gamma}_c\,, \end{cases}$$

where k and n denotes the consistency and power-law index, respectively. This regularization was done by defining a slope of original Bulkley model at the critical yield point $\dot{\gamma}_c$

$$\frac{d\mu}{d\dot{\gamma}}\Big|_{\dot{\gamma}=\dot{\gamma}_c} = -\frac{\tau_0}{\dot{\gamma}_c^2} + k(n-1)\dot{\gamma}_c^{n-2}\,.$$

The Herschel-Bulkley model is used to interpret the materials like dough, toothpaste, ketchup, mud, which need the initial yield stress. Fig. 2-5 describes the way how the shear stress τ and shear rate $\dot{\gamma}$ in Herschel-Bulkley model relate between each other. It is clear from the graph slope for $\dot{\gamma} < \dot{\gamma}_c$ starts from point $(0, \tau_0\frac{2}{\dot{\gamma}_c} + k(2-n))$ and at yield point $(\dot{\gamma}_c, \frac{\tau_0}{\dot{\gamma}_c} + k)$ behaviour of the fluid changes to Bingham model [8]. If $0 < n < 1$, the fluid possesses the property of the so-called shear thinning. The case $n > 1$ is known as fluid with shear thickening behaviour. In the case of $n = 1$ the fluid with the constant viscosity μ belongs to the class of Newtonian fluids.

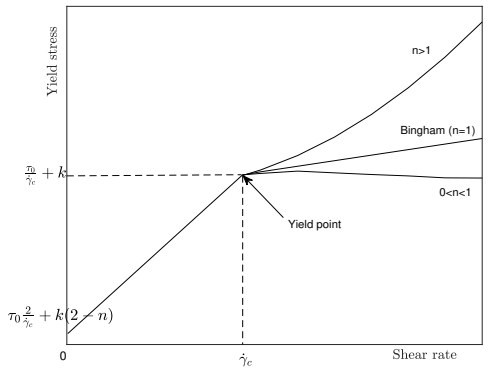

Figure 2-5: Dependence of shear rate stress with shear rate for modified Herschel-Bulkley model that was regularized by Tanner and Milthorpe [28]

Another well known regularization of Herschel-Bulkley model was presented by Papanastasiou [25]. His modification was done by substituting the apparent viscosity of the fluid by a function that can approximate the rheological behaviour, but keeps

the boundaries for any small value of $\dot{\gamma}$. This change was done by entering new parameter ε to apparent viscosity, which can describe the effect of the regularization. For large value of strain rate the viscosity aims to μ if parameter ε is high. The viscosity of the fluid produces high values which can lead to small rate of $\dot{\gamma}$ in the unyielded region, therefore the movement of solid body is approximated. In the case when shear rate tends to zero, the viscosity in (2.3) aims to the finite value $\varepsilon\tau_y + \mu$ instead of zero [27]. The proposed regularization, which is also called as *Bingham-Papanastasiou model* has the following form

$$\boldsymbol{\tau}(\dot{\boldsymbol{\gamma}}) = \left(\mu + \frac{\tau_y}{\dot{\gamma}}\left[1 - e^{-\varepsilon\dot{\gamma}}\right]\right)\dot{\boldsymbol{\gamma}} \quad \text{for all} \quad \dot{\gamma}\,, \tag{2.3}$$

where τ_y denotes the magnitude of the yield stress.

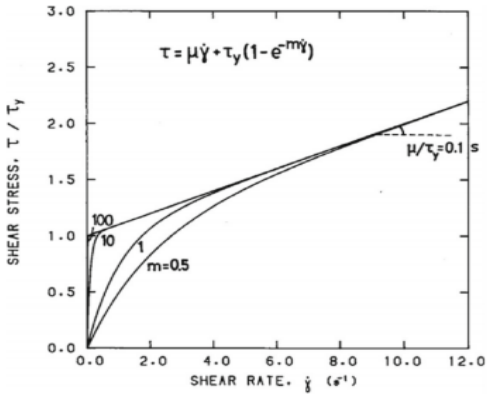

Figure 2-6: Variation of Shear Stress with Shear Rate For Bingham fluid according to *Bingham-Papanastasiou model* for several values of the regularization parameter ε [24]

Chapter 3

Navier-Stokes equations for 3D printing

The mathematical model for extrusion process will be considered in this chapter. The continuity and momentum equations in cylindrical coordinates will be presented and simplified in the case of axis symmetry for non-Newtonian fluids. Also, the equation of the motion of an incompressible fluids with non-Newtonian viscosity that depends on the pressure and shear rate of the paste will be formulated in this chapter.

3.1 Navies-Stokes equations

Fluid dynamics describes the motion of liquids and gases which seem to be continuous in structure by macroscopic research and whose unknown quantities like velocity and pressure fields are assumed to be continuous functions of the spatial coordinates and time. The Navier-Stokes equations are a set of nonlinear differential equations that describes the velocity and pressure of fluid. These equations can be used for simulations of weather, motion of the air in the atmosphere, water flow in tube, as well as plenty other fluid flow phenomena. The Navier-Stokes equations depend on time and consist of continuity equation for conservation of mass, conservation of momentum equations and conservation of energy equation.

Generally, the Navier-Stokes equations can be solved analytically in a closed form

only in a few cases. However, in some special cases the equations could be simplified and approached analytically. In the present study we consider incompressible, steady-state, laminar flow.

Incompressible fluid

The continuity equation in the case of incompressible fluid with no varying density implies $\nabla \cdot \boldsymbol{v} = 0$ where $\boldsymbol{v}$ denotes the velocity field. This formulation is used for the simplified model. In fact, all fluids are compressible up to a certain degree.

Steady flow

In the case of steady flow all changes of fluid properties with respect to the time are equal to zero. Steady flows are applicable to wide class of problems, like flow through a pipe, lift and drag on wing.

Laminar flow

The laminar flow is defined by fluid particles following smooth paths in layer where each layer moves smoothly past the adjoining layers without mixing. In the laminar flow the motion of the fluid is very ordered with particles cloud to solid surface flowing in straight lines parallel to that surface.

The mass in the control volume can not be produced or ruined according to physical laws. *The conservation of mass* which is also called *the continuity equation* describes the mass flow rate difference through system between inlet and outlet section is equal to zero, c.f. [34],

$$\frac{\partial \rho}{\partial t} + \rho(\nabla \cdot \boldsymbol{v}) = 0 \tag{3.1}$$

where ρ denotes the density, $\boldsymbol{v}$ stands for velocity and ∇ is the gradient operator

$$\nabla = \boldsymbol{i}\frac{\partial}{\partial x} + \boldsymbol{j}\frac{\partial}{\partial y} + \boldsymbol{k}\frac{\partial}{\partial z}\,. \tag{3.2}$$

Here, $\boldsymbol{i}$, $\boldsymbol{j}$ and $\boldsymbol{k}$ denote the canonical unit basis vectors in $\mathbb{R}^3$. The flow with constant density is assumed to be incompressible and therefore the continuity equation

is simplified [34] which specifies a steady-state process

$$\frac{\partial \rho}{\partial t} = 0 \implies \nabla \cdot \boldsymbol{v} = \frac{\partial v_1}{\partial x} + \frac{\partial v_2}{\partial y} + \frac{\partial v_3}{\partial z} = 0\,. \tag{3.3}$$

The momentum in a control volume is kept constant implying *conservation of momentum*. This is justified by Newton's Second Law of motion

$$\boldsymbol{F} = m\boldsymbol{a} \tag{3.4}$$

where $\boldsymbol{F}$ is the force that applied to any particle, m is the mass, $\boldsymbol{a}$ is the acceleration. In terms of density it means

$$\rho \frac{\partial \boldsymbol{v}}{\partial t} = \boldsymbol{f}_{body} + \boldsymbol{f}_{surface} \tag{3.5}$$

where $\boldsymbol{f}$ is the force acting on the fluid particle per unit volume, $\boldsymbol{f}_{body}$ is exerted on the whole mass of fluid particles

$$\boldsymbol{f}_{body} = \rho \cdot \boldsymbol{g} \tag{3.6}$$

where ρ stands for the density of the fluid and $\boldsymbol{g}$ is the gravitational acceleration. $\boldsymbol{f}_{surface}$ is defined by the sum of pressure and viscous forces

$$\boldsymbol{f}_{surface} = \nabla \cdot \tau_{ij} = \frac{\partial \tau_{ij}}{\partial x_i} = \boldsymbol{f}_{pressure} + \boldsymbol{f}_{viscous} \tag{3.7}$$

where τ_{ij} denotes the stress tensor. According to Stokes' law of Newtonian viscous fluid [34], τ_{ij} is formulated as:

$$\tau_{ij} = -p\delta_{ij} + \mu(\frac{\partial v_i}{\partial x_j} + \frac{\partial v_j}{\partial x_i}) \tag{3.8}$$

Newton's equation of motion could be established in the following form

$$\rho \frac{\partial \boldsymbol{v}}{\partial t} = \rho \cdot \boldsymbol{g} + \nabla \cdot \tau_{ij} \tag{3.9}$$

Consequently, we obtain the Navier-Stokes equations of Newtonian viscous fluid

$$\rho\frac{\partial \boldsymbol{v}}{\partial t} = \rho\boldsymbol{g} - \nabla p + \frac{\partial}{\partial x_i}\left[\mu\left(\frac{\partial v_i}{\partial x_j} + \frac{\partial v_j}{\partial x_i}\right)\right] . \tag{3.10}$$

In the case that density of fluid is constant, the equations are simplified with viscosity coefficient $\mu = constant$ for Newtonian fluid and $\nabla \cdot v = 0$. Therefore, The Navier-Stokes equations for an incompressible three-dimensional flow can be defined as

$$\rho\frac{\partial \boldsymbol{v}}{\partial t} = \rho\boldsymbol{g} - \nabla p + \mu\Delta\boldsymbol{v} . \tag{3.11}$$

3.2 Navier-Stokes equations in Cartesian coordinates

Let us consider Navier-Stokes equations for Newtonian fluid in Cartesian coordinate system with components of velocity vector $\boldsymbol{v} = (u, v, w)$ [35]. The continuity equation in the case of the external force $\boldsymbol{f} = (f_x, f_y, f_z)$ can be expressed as follows

$$\frac{\partial u}{\partial x} + \frac{\partial v}{\partial y} + \frac{\partial w}{\partial z} = 0 .$$

The momentum equations are given if the following form

u-momentum:

$$\rho\left(\frac{\partial u}{\partial t} + u\frac{\partial u}{\partial x} + v\frac{\partial u}{\partial y} + w\frac{\partial u}{\partial z}\right) = -\frac{\partial p}{\partial x} + \mu\left(\frac{\partial^2 u}{\partial x^2} + \frac{\partial^2 u}{\partial y^2} + \frac{\partial^2 u}{\partial z^2}\right) + f_x ,$$

v-momentum:

$$\rho\left(\frac{\partial v}{\partial t} + u\frac{\partial v}{\partial x} + v\frac{\partial v}{\partial y} + w\frac{\partial v}{\partial z}\right) = -\frac{\partial p}{\partial y} + \mu\left(\frac{\partial^2 v}{\partial x^2} + \frac{\partial^2 v}{\partial y^2} + \frac{\partial^2 v}{\partial z^2}\right) + f_y ,$$

w-momentum:

$$\rho\left(\frac{\partial w}{\partial t} + u\frac{\partial w}{\partial x} + v\frac{\partial w}{\partial y} + w\frac{\partial w}{\partial z}\right) = -\frac{\partial p}{\partial z} + \mu\left(\frac{\partial^2 w}{\partial x^2} + \frac{\partial^2 w}{\partial y^2} + \frac{\partial^2 w}{\partial z^2}\right) + f_z .$$

3.3 Navier-Stokes equations in cylindrical coordinates

The Navier-Stokes equations for Newtonian fluid in cylindrical coordinates (r, θ, z) for the velocity vector $\boldsymbol{v} = (v_r, v_\theta, v_z)$ [35] become the following form of continuity equation

$$\frac{1}{r}\frac{\partial v_r}{\partial r} + \frac{1}{r}\frac{\partial v_\theta}{\partial \theta} + \frac{\partial v_z}{\partial z} = 0\,,$$

and the momentum equations are given by

r-momentum:

$$\begin{aligned}&\frac{\partial v_r}{\partial t} + v_r\frac{\partial v_r}{\partial r} + \frac{v_\theta}{r}\frac{\partial v_r}{\partial \theta} + v_z\frac{\partial v_r}{\partial z} - \frac{{v_\theta}^2}{r}\\ &= -\frac{1}{\rho}\frac{\partial p}{\partial r} + \mu\left[\frac{1}{r}\frac{\partial}{\partial r}\left(r\frac{\partial v_r}{\partial r}\right) + \frac{1}{r^2}\frac{\partial^2 v_r}{\partial \theta^2} + \frac{\partial^2 v_z}{\partial z^2} - \frac{v_r}{r^2} - \frac{2}{r^2}\frac{\partial v_\theta}{\partial \theta}\right] + f_r\,,\end{aligned}$$

θ-momentum:

$$\begin{aligned}&\frac{\partial v_\theta}{\partial t} + v_r\frac{\partial v_\theta}{\partial r} + \frac{v_\theta}{r}\frac{\partial v_\theta}{\partial \theta} + v_z\frac{\partial v_\theta}{\partial z} - \frac{v_r v_\theta}{r}\\ &= -\frac{1}{\rho}\frac{\partial p}{\partial \theta} + \mu\left[\frac{1}{r}\frac{\partial}{\partial r}\left(r\frac{\partial v_\theta}{\partial r}\right) + \frac{1}{r^2}\frac{\partial^2 v_\theta}{\partial \theta^2} + \frac{\partial^2 v_\theta}{\partial z^2} - \frac{v_\theta}{r^2} - \frac{2}{r^2}\frac{\partial v_r}{\partial \theta}\right] + f_\theta\,,\end{aligned}$$

z-momentum:

$$\begin{aligned}&\frac{\partial v_z}{\partial t} + v_r\frac{\partial v_z}{\partial r} + \frac{v_\theta}{r}\frac{\partial v_z}{\partial \theta} + v_z\frac{\partial v_z}{\partial z}\\ &= -\frac{1}{\rho}\frac{\partial p}{\partial z} + \mu\left[\frac{1}{r}\frac{\partial}{\partial r}\left(r\frac{\partial v_z}{\partial r}\right) + \frac{1}{r^2}\frac{\partial^2 v_z}{\partial \theta^2} + \frac{\partial^2 v_\theta}{\partial z^2}\right] + f_z\,.\end{aligned}$$

3.4 Nondimensionalization

Rewriting the Navier-Stokes equations in cylindrical coordinate system in the dimensionless form simplifies the equations and underlines the most important parameters. At first we choose characteristic values defining the flow, like characteristic velocity V represents the fluid velocity in the flow domain, characteristic length L defines the length over which velocity is changing proportional to characteristic velocity V, characteristic pressure p_∞ and temperature T in the case of non-isothermal fluid [36]. During nondimensionalization of governing equations, the structure of the Navier-Stokes equations generally leads to the definition of the Reynolds number. Let us

introduce the dimensionless parameters for Navier-Stokes equations in the radial and longitudinal directions as follows

$$r^* = \frac{r}{L}, \quad z^* = \frac{z}{L}, \quad v_r^* = \frac{v_r}{V}, \quad v_z^* = \frac{v_z}{V}, \quad p^* = \frac{pL}{\mu_{eff} V}, \quad Re = \frac{\rho V L}{\mu_{eff}}. \tag{3.12}$$

The dimensionless form of governing equations can be achieved by using these substitutions. For instance, the momentum equations in r and z directions for the incompressible steady-state flow of Newtonian fluid can be converted in the following way

r-momentum:

$$\rho\left(v_r\frac{\partial v_r}{\partial r} + v_z\frac{\partial v_r}{\partial z}\right) = -\frac{\partial p}{\partial r} + \rho g_r + \mu\left[\left(\frac{1}{r}\frac{\partial}{\partial r}\left(r\frac{\partial v_r}{\partial r}\right)\right) - \frac{v_r}{r^2} + \frac{\partial^2 v_r}{\partial z^2}\right]$$

z-momentum:

$$\rho\left(v_r\frac{v_z}{\partial r} + v_z\frac{\partial v_z}{\partial z}\right) = -\frac{\partial p}{\partial z} + \rho g_z + \mu\left[\frac{1}{r}\frac{\partial}{\partial r}\left(r\frac{\partial v_z}{\partial r}\right) + \frac{\partial^2 v_z}{\partial z^2}\right].$$

Reynolds number defines the ratio between the diffusive and convective terms of momentum equations. The value of Re determines whether the convection or diffusion dominates. Nondimensionalization is useful to get a deeper understanding of the relative size of the different terms presented in the Navier-Stokes equations. Identification of smaller terms in the equation is relevant for the proper choice of dimensionless parameters for scaling process. In our case the nondimensionalized Navier-Stokes equations without heat transfer depends on Reynolds number.

3.5 Navier-Stokes equation in axial symmetry

In the case of axial symmetric flows, the velocity in θ direction is constant and can be neglected [33]. In the following, the ram extruder for ceramic paste is elaborated as an axisymmetric model. If the pressure of the fluid p and the cylindrical velocity components $\boldsymbol{v} = (v_r, v_\theta, v_z)$ of Navier-Stokes equations are independent of the angular variable θ, then flow is called axisymmetric.

Navier-Stokes equations for steady, laminar, incompressible flow of non-Newtonian fluid in cylindrical coordinates in radial and longitudinal directions are formulated in the following form [1]

$$\begin{aligned} v_r\frac{\partial v_r}{\partial r}+v_z\frac{\partial v_z}{\partial z} &= f_r-\frac{1}{\rho}\frac{\partial p}{\partial r}+\frac{1}{\rho r}\frac{\partial}{\partial r}(r\tau_{rr})-\frac{1}{\rho}\frac{\tau_{rr}}{r}+\frac{1}{\rho}\frac{\partial \tau_{rz}}{\partial z}\,, \\ v_r\frac{\partial v_z}{\partial r}+v_z\frac{\partial v_z}{\partial z} &= f_r-\frac{1}{\rho}\frac{\partial p}{\partial z}+\frac{1}{\rho r}\frac{\partial}{\partial r}(r\tau_{rz})+\frac{1}{\rho}\frac{\partial \tau_{zz}}{\partial z}\,, \\ \frac{1}{r}\frac{\partial}{\partial r}(rv_r)+\frac{\partial v_z}{\partial z} &= 0\,, \end{aligned} \tag{3.13}$$

where v_r and v_z are the components of the velocity $\boldsymbol{v}=(v_r,v_z)$ in r and z directions. In (3.13) the expressions $\tau_{rz}=\mu(\dot{\gamma})$ and $\dot{\gamma}=\frac{\partial v_z}{\partial r}$ are identical with the stress tensor and shear rate in Herschel-Bulkley model for Bingham plastics. The analytical solutions for fully developed flow have been obtained for example in [1], i.e., $v_r=0$, $\frac{\partial v_z}{\partial z}=0$ and $\frac{\partial \tau_{zz}}{\partial z}=0$.

3.6 Governing model equations for the ceramic paste extrusion

The Navier-Stokes equations for an incompressible, non-Newtonian fluid are defined in the material domain $\Omega\subset R^d$ as [37]:

$$\begin{aligned} \rho\frac{\partial \boldsymbol{v}}{\partial t}-\nabla\cdot\boldsymbol{\tau}(\dot{\boldsymbol{\gamma}})+\rho(\boldsymbol{v}\cdot\nabla)\boldsymbol{v}+\nabla p &= \boldsymbol{f} \\ \nabla\cdot\boldsymbol{v} &= 0 \end{aligned} \tag{3.14}$$

where $\boldsymbol{v}$ and p are unknown velocity and pressure, ρ defines the density of the fluid, $\boldsymbol{f}$ is the bulk force. Note that $\boldsymbol{\tau}$ depends on the symmetric part of velocity gradient $\dot{\boldsymbol{\gamma}}=2\,\boldsymbol{D}\boldsymbol{v}=\nabla\boldsymbol{v}+\nabla\boldsymbol{v}^T$.

Model assumptions

(i) Due to low extrusion velocity and high viscosity of the fluid, the Reynolds Number will have small value, thus the flow is considered as laminar.

(ii) The developing section of the fluid flow is quiet short, because of small Reynolds number, we assume that flow is fully developed.

(iii) The extrusion die is totally filled by ceramic paste

(iv) The paste is taken as an incompressible.

(v) The fluid temperature is constant. Hence, the viscosity is presented as a function of shear rate and density depends only on pressure.

(vi) There is no slip on the wall, therefore the velocity of the fluid at the wall is equal to zero.

(vii) The pressure at the outlet of the extrusion die is 101325 Pa, that is 1 atm.

The initial conditions to model equation (3.14) are given as

$$\boldsymbol{v}(0,\cdot) = \boldsymbol{v}_0 \quad \text{in} \quad \Omega\,, \tag{3.15}$$

and the no-slip boundary condition

$$\boldsymbol{v}|_{\Gamma_w} = 0, \tag{3.16}$$

for all $t > 0$ from the considered time interval. Other types of boundary conditions are also relevant for extrusion, e.g., the outlet boundary condition. The momentum equation in isothermal case reads as follows [2]

$$\rho\left(\frac{\partial \boldsymbol{v}}{\partial t} + (\boldsymbol{v}\cdot\nabla)\boldsymbol{v}\right) - \nabla\cdot\boldsymbol{\sigma} = \boldsymbol{f} \tag{3.17}$$

The stress tensor can be defined as a combination of the volumetric and deviatoric stresses in the following way

$$\boldsymbol{\sigma} = -p\boldsymbol{I} + \boldsymbol{\tau} \tag{3.18}$$

where the deviatoric stress $\boldsymbol{\tau}$ is given as

$$\boldsymbol{\tau} = -p\boldsymbol{I} + \mu(\dot{\gamma})\dot{\boldsymbol{\gamma}},. \tag{3.19}$$

Here, μ represents the dynamic viscosity of the fluid that depends of the equivalent strain rate $\dot{\boldsymbol{\gamma}}$. The viscosity depends on the deformation process in case of non-Newtonian fluid. To this end, different models for viscoplastic fluids have been established. In this study, we consider the Herschel-Bulkley model (2.2), which combines the yield stress τ_0 with power-law model for viscosity [33]. The deviatoric stress tensor is given as

$$\begin{aligned} \boldsymbol{\tau}(\dot{\boldsymbol{\gamma}}) = \left(k\dot{\gamma}^{n-1} + \frac{\tau_0}{\dot{\gamma}}\right)\dot{\boldsymbol{\gamma}} \quad &\text{if} \quad \tau \geq \tau_0\,, \\ \dot{\boldsymbol{\gamma}} = \mathbf{0} \quad &\text{if} \quad \tau < \tau_0\,. \end{aligned} \tag{3.20}$$

where $\tau = \sqrt{\frac{1}{2}\boldsymbol{\tau} : \boldsymbol{\tau}}$. When the rate of deformation approaches to zero, there is a singularity in equation (3.20). Instead of solving the model equations numerically, we consider the regularized version of the Herschel-Bulkley model [51], which were described in Section 2.3

$$\mu(\dot{\gamma}) = \begin{cases} \frac{\tau_0}{\dot{\gamma}} + k\left(\frac{\dot{\gamma}}{\dot{\gamma}_c}\right)^{n-1} & \text{for} \quad \dot{\gamma} > \dot{\gamma}_c\,, \\ \tau_0 \frac{(2-\dot{\gamma}/\dot{\gamma}_c)}{\dot{\gamma}_c} + k\left[(2-n) + (n-1)\frac{\dot{\gamma}}{\dot{\gamma}_c}\right] & \text{for} \quad \dot{\gamma} < \dot{\gamma}_c\,. \end{cases}$$

Let us apply non-dimensional parameters to regularized Herschel-Bulkley model

$$\dot{\gamma}^* = \frac{L}{V}\dot{\gamma}\,, \quad Bn = \frac{\tau_0 \cdot L}{\mu_{eff} V}\,, \quad k^* = \frac{k}{\mu_{eff}}\,, \quad \tau^* = \frac{\tau L}{\mu_{eff} V}\,.$$

Here, Bn denotes the dimensionless parameter *Bingham number* which is used to study the flow of Bingham plastics. The value of Bn is defined as a ratio of yield stress and characteristic length to characteristic velocity and viscosity of the fluid [26]. In the following, we omit the asterisk notation. The dimensionless form of regularized Herschel-Bulkley model is reduced to

$$\boldsymbol{\tau}(\dot{\boldsymbol{\gamma}}) = \begin{cases} \left(\frac{Bn}{\dot{\gamma}} + k\frac{\dot{\gamma}^{n-1}}{\dot{\gamma}_c^{n-1}}\right) \cdot \dot{\boldsymbol{\gamma}} & \text{for } \dot{\gamma} \geq \dot{\gamma}_c\,, \\ \left(\left(\frac{2Bn}{\dot{\gamma}_c} + k(2-n)\right) + \left(k\frac{(n-1)}{\dot{\gamma}_c} - \frac{Bn}{\dot{\gamma}_c^2}\right) \cdot \dot{\gamma}\right) \cdot \dot{\boldsymbol{\gamma}} & \text{for } \dot{\gamma} < \dot{\gamma}_c\,. \end{cases}$$

The system of equations modeling the problem are given as follows

$$
\begin{aligned}
&v_r\frac{\partial v_r}{\partial r}+v_z\frac{\partial v_z}{\partial z}=f_r-\frac{1}{\rho}\frac{\partial p}{\partial r}+\frac{1}{\rho r}\frac{\partial}{\partial r}(r\tau_{rr})-\frac{1}{\rho}\frac{\tau_{rr}}{r}+\frac{1}{\rho}\frac{\partial \tau_{rz}}{\partial z}\,,\\
&v_r\frac{\partial v_z}{\partial r}+v_z\frac{\partial v_z}{\partial z}=f_r-\frac{1}{\rho}\frac{\partial p}{\partial z}+\frac{1}{\rho r}\frac{\partial}{\partial r}(r\tau_{rz})+\frac{1}{\rho}\frac{\partial \tau_{zz}}{\partial z}\,,\\
&\frac{1}{r}\frac{\partial}{\partial r}(rv_r)+\frac{\partial v_z}{\partial z}=0\,,\\
&\boldsymbol{\tau}(\dot{\boldsymbol{\gamma}})=\begin{cases}\left(\frac{Bn}{\dot\gamma}+k\frac{\dot\gamma^{n-1}}{\dot\gamma_c^{n-1}}\right)\cdot\dot{\boldsymbol{\gamma}} & \text{for } \dot\gamma\geq\dot\gamma_c\,,\\ \left(\left(\frac{2Bn}{\dot\gamma_c}+k(2-n)\right)+\left(k\frac{(n-1)}{\dot\gamma_c}-\frac{Bn}{\dot\gamma_c^2}\right)\cdot\dot\gamma\right)\cdot\dot{\boldsymbol{\gamma}} & \text{for } \dot\gamma<\dot\gamma_c\end{cases}
\end{aligned}
\tag{3.21}
$$

subject to the initial and no-slip and outflow boundary conditions. Due to the complexity of Navier-Stokes equations for the ceramic paste extrusion it is almost impossible to solve them analytically. Hence, we are going to apply an appropriate numerical method for the fluid flow problems. In the next chapter we introduce the finite element method by which the solution to the above system of model equations can be approximated numerically.

Chapter 4

Numerical methods

4.1 Computational Fluid Dynamics

Fluid flow problems are usually defined by partial differential equations whose analytical solution can be established in closed form only in special cases. To find approximate solutions numerically, we use *discretization methods* which lead to systems of algebraic equations whose solutions can be obtained using iterative methods and computers. Generally a solution method is determined for a specific model problem and set of equations. The next step is selecting an appropriate discretization method, that is a method to approximate the set of differential equations by a system of algebraic equations for a variables at the set of discrete locations in space. Among the various approaches, the most common in fluid dynamics are Finite Difference Method (FDM), Finite Volume Method (FVM) and Finite Element method (FEM) [29].

4.2 Finite Element Method

The idea of 'finite elements' can be tracked back to the approaches that were used in evaluation of stress in solid mechanics. The structure is divided into tiny bases of different shape and collected again after analysis of every 'element' of the structure. This method was improved and regular development led to the foundation of *Finite Element Method*.

The space discretization is characterized by a set of units, which we call elements in FEM and it is in contrast to the number of points in *Finite Difference Methods*. In Finite Element Method the domain consist of the set of finite elements that are usually unstructured. In 2D problems those elements are mostly triangles or quadrilaterals and in 3D there are tetrahedral or hexahedra. Finite Element method assumes an integral formulation as the first stage which can be taken into account as a generalization of the *Finite Volume Methods* [29]. The characteristic feature of Finite Element Methods is the fact that the equations are multiplied by a weight functions and then integrated over the entire domain. The number of unknown function values at each

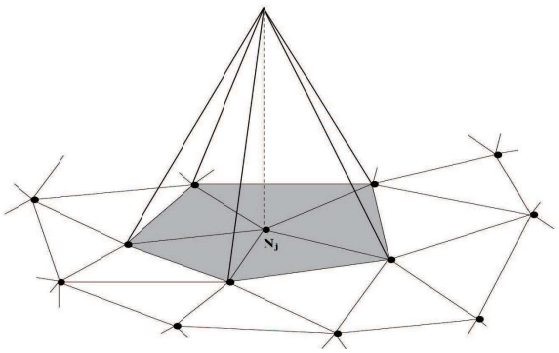

Figure 4-1: A global piecewise linear finite element basis function defined over the triangular mesh.

node and their derivatives are usually called the *degrees of freedom* or *nodal values* of the numerical problem. The field variables can be approximated by linear combinations of ***shape functions, interpolation functions or trial functions*** [39]. An example of a global finite element shape function defined over the triangular mesh is presented in Fig. 4-1. In our model we will use the following ansatz for the finite element velocity and pressure approximations

$$\boldsymbol{v}_h(\boldsymbol{x}) = \sum_{j=1}^{N_h} v_j \varphi_j(\boldsymbol{x})\,, \qquad p_h(\boldsymbol{x}) = \sum_{j=1}^{M_h} p_j \psi_j(\boldsymbol{x})\,,$$

where for the standard Galerkin method to produce a well-posed discrete algebraic

system, we have to satisfy $M_h < N_h$. Moreover, a discrete *inf–sup* stability condition restricts the choice of the finite element velocity and pressure spaces for the finite element approximations of the velocity and pressure unknowns. An *inf-sup* stable pairs of approximation spaces for velocity and pressure can be constructed by using lower degree basis functions or coarser mesh for the pressure. Notice that the use of equal-order interpolations for the velocity and pressure lead to oscillatory solutions unless stabilization terms are added to the discrete continuity equations. [58–60]

Integral formulation can be achieved from system of differential equation via ***weak formulation*** or in other words the ***method of weighted residuals***. In the case of simple finite element methods, the solution can be approximated using a linear shape functions in each element such that it provides continuity of the solution through the boundaries of elements. Such a linear shape function can be defined from its values at the vertices of the elements [39]. Next step is to substitute this approximation into the weighted integral of conservation law. The best discrete solution is chosen in the set of allowed functions (that is with minimum residual). One of meaningful advantage of Finite Element methods is the opportunity to deal with various geometries. The grids can be easily refined, every element is divided into sub-elements in a certain way. Finite Element methods are suitable to analyze numerically and can show the optimality features for specific type of equations. The main disadvantage compared to any other method is that matrices of linearized equations are not well organized as for regular grids, which makes it difficult to find effective solution approach in the general case of coupled model equations.

4.2.1 Variational formulation

The finite element discretization of the Navier-Stokes problem for Herschel-Bulkley fluid is related to the variational formulation which was for the first time proposed by Duvaut-Lions [43]. Let us now introduce the notations. Let $\Omega = (0, L)^d$, $L \in (0, \infty)$ be a cube in R^d, $d = 2, 3$ with boundary $\partial\Omega$ and $\Gamma_j = \partial\Omega \cap \{x_j = 0\}, \Gamma_{j+d} = \partial\Omega \cap \{x_j = L\}$ for $j = 1, ..., d$. For $T > 0$ Q_T is the time-space cylinder $I \times \Omega$, where $I = (0, T)$ is a time interval. By $(L^r(\Omega), \|\cdot\|_r)$ and $(W^{k,r}(\Omega), \|\cdot\|_{k,r})$ we specify the

Sobolev spaces of periodic functions [30]. Due to incompressible condition $\nabla \cdot \boldsymbol{v} = 0$ we also define the spaces of divergence free functions

$$\mathcal{V} = \{\boldsymbol{\psi} \in C^{\infty}_{per}(\Omega)^d : \quad \nabla \boldsymbol{\psi} \cdot = 0\},$$

and

$$H = \text{ closure of } \mathcal{V} \quad \text{w.r.t.} \quad L^2(\Omega)^d - \text{ norm},$$

$$V_r = \text{ closure of } \mathcal{V} \quad \text{w.r.t.} \quad W^{1,r}(\Omega)^d - \text{seminorm},$$

where $r \in (1, \infty)$.

We say that the vector function $\boldsymbol{v}(\boldsymbol{x}, t)$ is a *weak solution* of Navier-Stokes equations on $[0, T)$ for $p \in (1, 2]$ [30] if

$$\boldsymbol{v} \in L^{\infty}(I; H) \cap L^{p}(I; V_p) \tag{4.1}$$

for all $t \in I$ and all $\boldsymbol{\phi} \in \mathcal{V}$ satisfies

$$\int_{\Omega} \rho \frac{\partial \boldsymbol{v}}{\partial t} \cdot \boldsymbol{\phi}\, dx + \int_{\Omega} \boldsymbol{\tau}(\boldsymbol{D}(\boldsymbol{v}), \boldsymbol{v}) \cdot \boldsymbol{D}(\boldsymbol{\phi})\, dx + \int_{\Omega} \rho(\boldsymbol{v} \cdot \nabla)\boldsymbol{v} \cdot \boldsymbol{\phi}\, dx = \int_{\Omega} \boldsymbol{f} \cdot \boldsymbol{\phi}\, dx\,. \tag{4.2}$$

The existence and stability of solution for fluids with non-Newtonian viscosity has been proved by Malek and Rajagopal [30]. Authors proposed new approaches for stability of the rest state of shear dependent fluids for any initial conditions. Notice, that the reconstruction of the weak pressure follows using an appropriate choice of the pressure space due to the *Ladyzhenskaya-Babushka-Brezzi* inf-sup condition. Also, there is presented a discussion regarding the existence and regularity of solutions to such a problem with small data. The equations for non-stationary Herschel-Bulkley fluid were also studied by H. Eberlein and M. Ruzicka in [31] where the existence of weak solution to the problem was proved. Equations (3.21) are at the centre of modeling of ceramic paste flows. Solving these equations for a specific set of boundary conditions, i.e. inlet, outlet and wall of the extruder, determines the velocity and the pressure of the fluid in a extruder domain. Navier-Stokes equations can be solved

analytically only in a very few cases. Therefore, appropriate numerical schemes have to be applied. The common practice in engineering and scientific computing is to study Navier-Stokes equations via simulation and use of advanced software.

4.3 COMSOL - Multiphysics Software Package for Computational Fluid Dynamics

COMSOL Multiphysics software allows to compute approximate solutions of coupled equations from physics, for example, fluid momentum transfer with heat transfer models can be created for the same body and solved numerically at the same time. COMSOL is a software for simulation of physics in which Partial Differential Equations are approximately solved using Finite Element Methods. COMSOL Multiphysics is able to generate 1D, 2D and 3D models where one can define geometry of the domain, physics with all required equations and boundary conditions, and specify the mesh and visualize the results using solely this software. The *Computational Fluid Dynamics* (CFD) Module is a standard package which serves COMSOL Multiphysics software for modeling environment with specialized physics interfaces and processes optimized for the analysis of any type of fluid flows.

In this study the *Laminar Flow* interface in CFD was used for computation of fluid velocity and pressure for a steady-state fluid based on the modified Herschel-Bulkley model. A flow of the fluid is considered as laminar if the Reynolds number is lower than a specific critical value. This critical value of Reynolds number depends on the concrete model. The Navier-Stokes equations (3.21) including conservation of momentum equations are solved in the laminar flow regime. The physics interface supports flows of non-Newtonian type which is in our case the *Modified Herschel-Bulkley model* presented in the previous chapter. The *Volume Force* defines applied volume force of the fluid, which is on the right-hand side of the governing momentum equation (3.21). The parameters of the force corresponds to those from [2]. There is only one vertical component and the force is taken per volume.

In this study, we will use the laminar flow module of CFD in COMSOL software to produce simulations of extrusion process of alumina paste. To this end, first we need to build a new geometry of the die with axis symmetry to reduce the number of degrees of freedom and consequently the computation time. Authors in [2] and [41] have done similar simulations of extrusion using COMSOL software but for the different die geometry. In this research, continuous piecewise quadratic approximation for the velocity and continuous linear approximation for the pressure was used, which is also known as Taylor-Hood element [59]. In the next step, all required parameters in laminar flow physics will be set. The boundary conditions will be specified at the inlet, outlet and wall of the die. Mesh of the extrusion dies was built by linear triangular elements. Also, the input data for the modified Herschel-Bulkley model for alumina paste will be defined. Using the idea of finite element approach, we need to construct an appropriate mesh for a die which is represented in axis symmetric case by a two-dimensional domain. The COMSOL software computes the finite element solution to the fluid model problem and produces graphical results that describe velocity, pressure and shear rate of the paste. The simulation results of lid-driven cavity flow problem, non-Newtonian fluid flow in cylindrical pipe, pressure driven flow in pipe are presented in the next section.

4.4 Lid-driven cavity flow

The lid-driven cavity is a standard CFD problem for Newtonian and non-Newtonian incompressible fluid flows. We consider square cavity which consists of tree solid walls with no-slip boundary condition and lid-driven top wall with tangential unit velocity, see Fig. 4-2(a). Let us consider the dimensionless Navier-Stokes equations

$$(\boldsymbol{v} \cdot \nabla)\boldsymbol{v} = -\nabla p + \frac{1}{Re}\Delta \boldsymbol{v} \tag{4.3}$$

where Re is the Reynolds number which is defined as $Re = \frac{\rho U L}{\mu}$. Here, U denotes the magnitude of the characteristic velocity, and L stands for the characteristic length. As

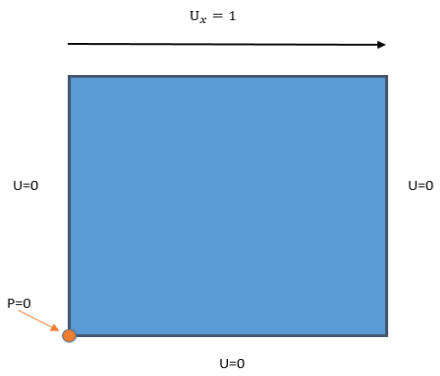

(a) The boundary conditions for the square cavity problem.

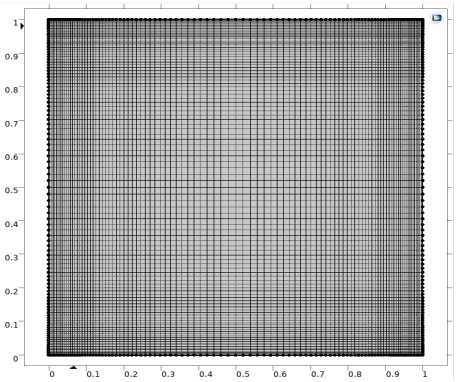

(b) Mapped mesh for the lid-driven cavity model.

Figure 4-2: The boundary conditions for the square cavity problem and the mesh used for simulations.

Reynolds number grows, the inertial term becomes more significant then the viscous term of the equation. We see that the inertial term in equation is nonlinear, however viscous term is linear, so the cavity problem becomes more nonlinear as Reynolds number increasing. To demonstrate nonlinear ramping for this problem we perform auxiliary sweep for various Reynolds numbers. In this way we can compare the velocity and pressure profiles for multiple Reynolds numbers. The problem is steady-state, without inlet or outlet, where pressure could be defined. There is a reference pressure point 0 at the lower left corner of the square, and it fits to an absolute pressure of 1 atm.

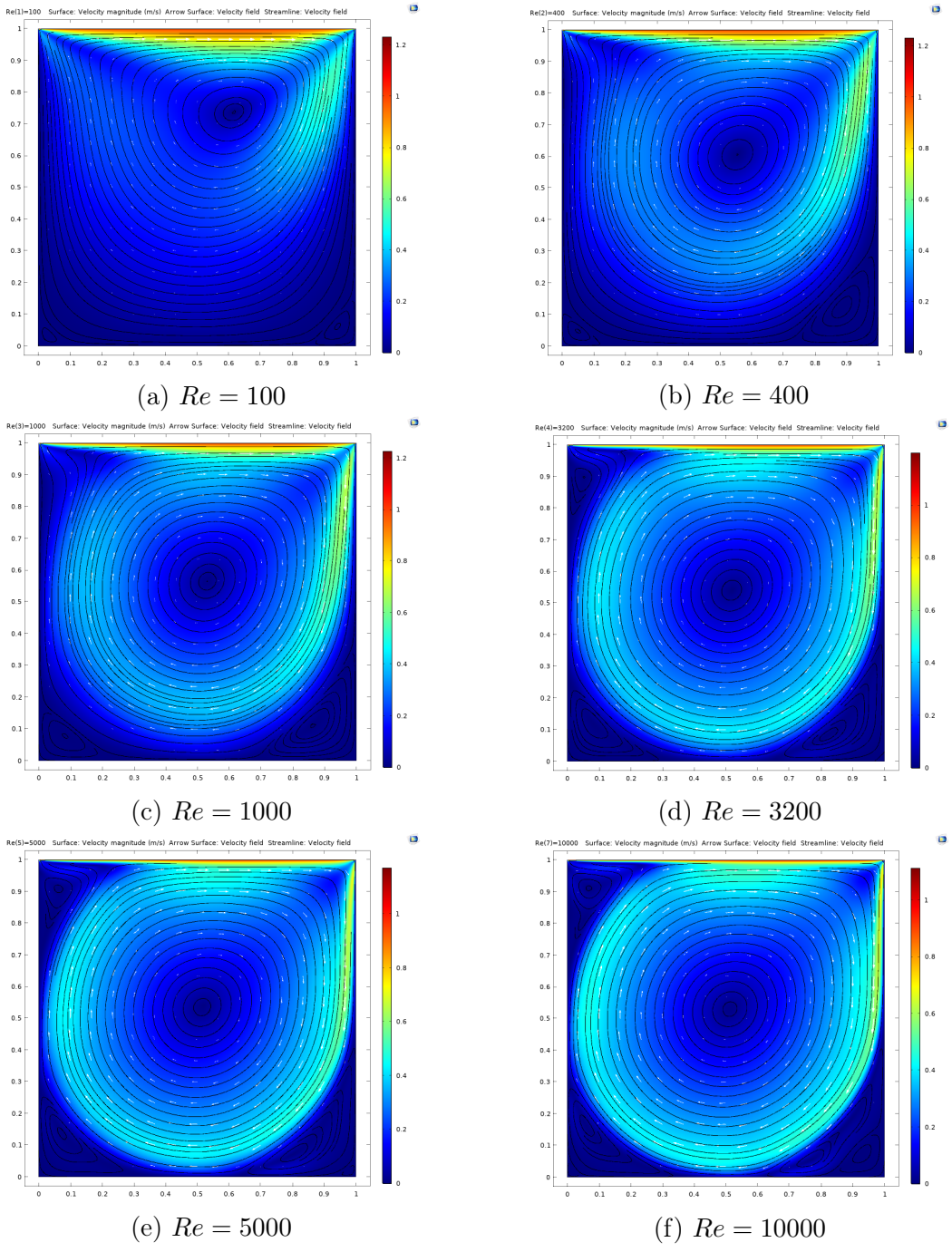

(a) $Re = 100$ (b) $Re = 400$

(c) $Re = 1000$ (d) $Re = 3200$

(e) $Re = 5000$ (f) $Re = 10000$

Figure 4-3: The velocity fields for the lid-driven cavity flow problem and various Reynolds numbers.

The mapped mesh was used to discretize the domain of the square cavity, see Fig. 4-2(b). For this type of problem we use adaptive elements near the no-slip walls where boundary layers may occur which is essential for solving the algebraic systems for larger Reynolds numbers. Fig. 4-3 shows the velocity profiles for the lid

driven cavity flow problem for different values of Reynolds number (100, 400, 1000, 3200, 5000, 10000). In each case one can observe that the velocity is approaching 1 close to the top wall and 0 at walls with no-slip and bottom side. Streamlines show that central vortex spins faster for higher value of Reynolds number since inertial force of the fluid flow is increasing. There are regions with the low velocity in the left corners and bottom side of the square where secondary vortexes occur. Fig. 4-4 shows the velocity profiles for the flow in the square cavity along a horizontal and vertical line which pass through the center of cavity. By using auxiliary sweep in COMSOL Multiphysics we can measure velocity profiles for different values of Re. Note that this software does not show error for high Reynolds number. The graph of velocity profile along the horizontal line starts from zero and ends up at zero value due to no-slip boundary condition ($\boldsymbol{v} = \mathbf{0}$). There is significant growth of velocity on the left and right sides where is the central vortex region, see Fig. 4-3. A similar effect is for the velocity profiles along the vertical line. The velocity graph starts growing from zero value (at the bottom side $\boldsymbol{v} = \mathbf{0}$) and passes through the vortex flow reaching the value 1 at the top wall.

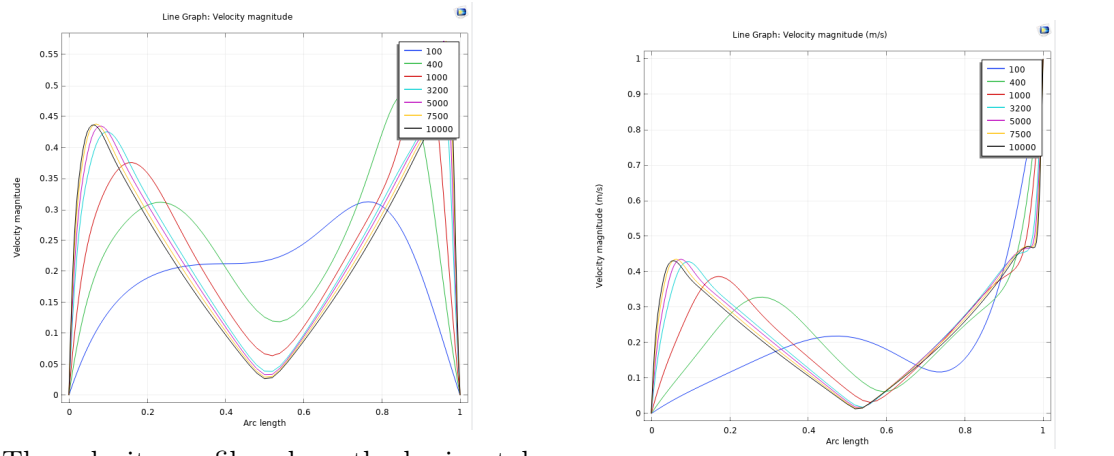

(a) The velocity profiles along the horizontal line.

(b) The velocity profiles along the vertical line.

Figure 4-4: The velocity profiles for the lid-driven cavity flow problem along the horizontal and vertical cut lines for various Reynolds numbers.

Fig. 4-5 illustrates the pressure profiles for the lid-driven cavity flow model for various Reynolds number. The pressure curve smoothly decreases in the middle of

the cavity and increases up to the same value for the case where the pressure was plotted along the horizontal line passing through the center of the square. The similar picture we got for the pressure along the vertical line except that the initial pressure value was almost zero, gradually decreasing till the center point and increasing only up to -0.06 Pa. The profiles were prepared for different values of the Reynolds number Re such that the difference of profiles corresponding to the small and higher values of Re can be observed.

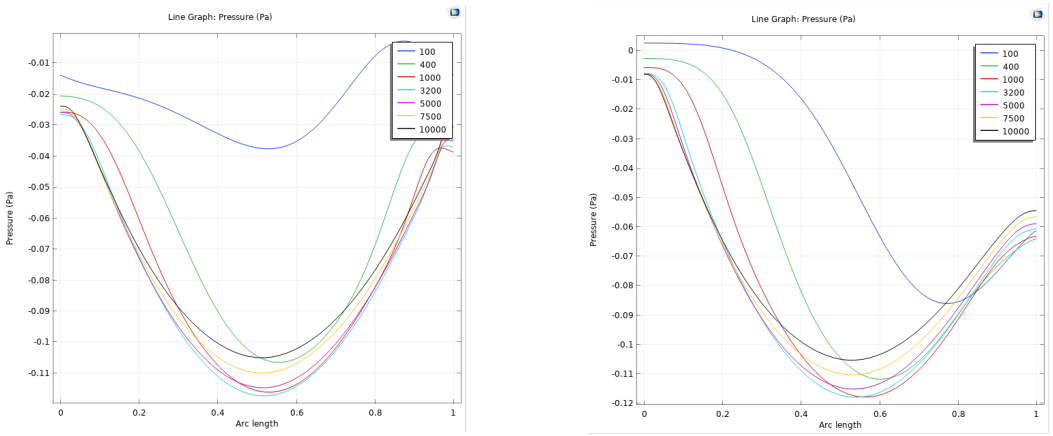

(a) The pressure along the horizontal line. (b) The pressure along the vertical line.

Figure 4-5: The pressure profiles for the lid-driven cavity flow problem along the horizontal and vertical cut lines for various Reynolds numbers.

4.4.1 The Herschel-Bulkley model for the lid-driven cavity flow

The modified Herschel-Bulkley model in dimensionless form is considered for the lid-driven cavity flow problem. The dimensionless form of the Bingham plastic viscosity depends only on the Bingham number. In this section the parameter study for various Bingham numbers is performed. The velocity and pressure profiles along the horizontal and vertical lines passing through the center are presented. E. Mitsoulis and Th. Zisis in [42] have studied flow of Bingham plastics in a lid-driven square cavity applying regularized Bingham-Papanastasiou model.

Fig. 4-6 illustrates the velocity profile along the horizontal and vertical centerlines for the modified Herschel-Bulkley model and different values of the Bingham number. The velocity along the horizontal line rapidly grows up to 0.22 m/s with a small decline

in the center region and decreases to zero value at the no-slip wall. The velocity along the vertical cut line starting from zero velocity slightly increases in the middle of the square cavity, passes the vortex region and reaches its maximum value of 1 m/s at the top wall. In general, the curve of the velocity for the Herschel-Bulkley model is similar to the velocity profile in standard case of the lid-driven flow, see Fig. 4-4. In Fig. 4-6(a)-(c) there is no significant difference between profiles corresponding to various Bingham numbers. However, the zoomed image shows the slight changes in velocity profiles for various Bn number. In other words, the change in velocity is not significant for various Bingham numbers. The pressure profiles for the modified Herschel-Bulkley

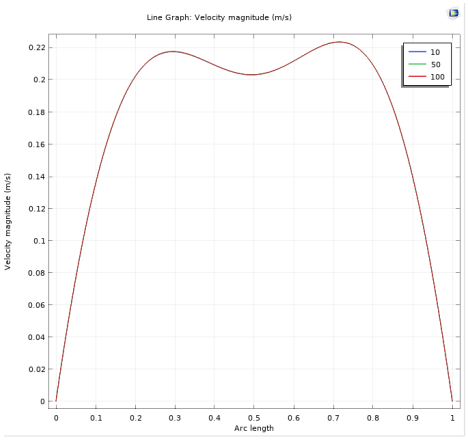

(a) The velocity along the horizontal centerline.

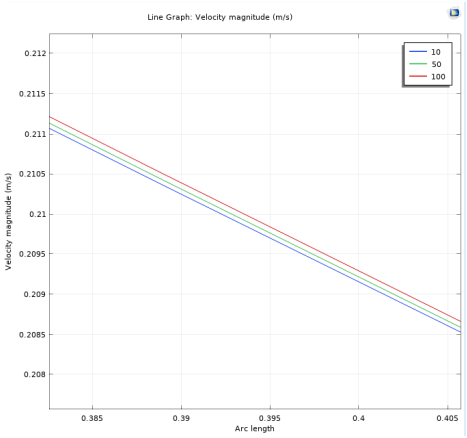

(b) The zoomed velocity profiles.

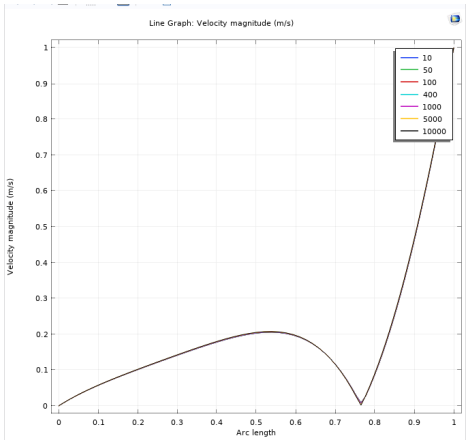

(c) The velocity along the vertical centerline.

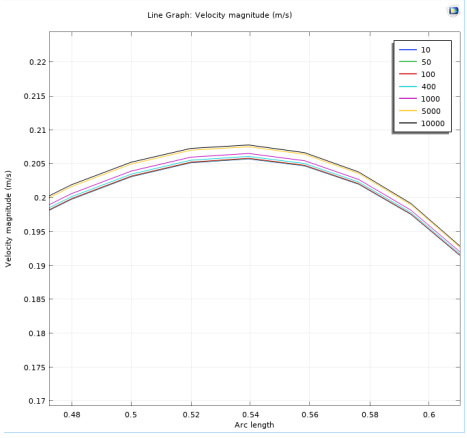

(d) The zoomed velocity profile.

Figure 4-6: The velocity profiles for the Herschel-Bulkley viscosity model applied to the lid-driven cavity flow problem and their zoomed parts.

model are also studied for various Bingham numbers. The shape of the pressure curve

for this case, see Fig. 4-7, is similar to Fig. 4-5. Clearly, the increasing Bn number strongly affects the curve amplitude, i.e., the higher the Bingham number the higher pressure value.

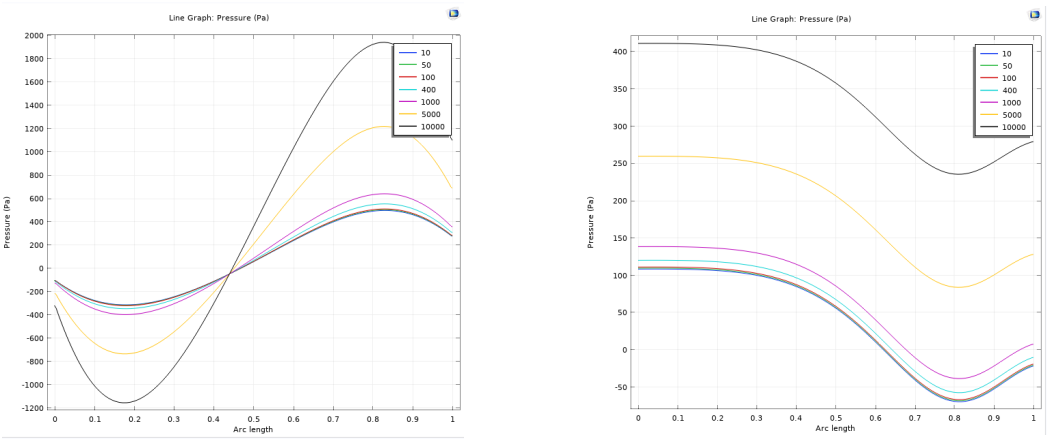

(a) The pressure along the horizontal line.

(b) The pressure along the vertical line.

Figure 4-7: Plots of pressure profiles for the Herschel-Bulkley model applied to the lid-driven cavity flow problem presented along the horizontal and vertical centerlines.

4.4.2 Newtonian and non-Newtonian fluids for lid-driven cavity flow model

In previous section we have studied the modified Herschel-Bulkley model applied to the cavity flow problem. Let us consider a simple Newtonian fluid flow and compare it to the Herschel-Bulkley model.

The plots presented in Fig. 4-8 show the velocity profiles for the Newtonian fluid (a) and the modified Herschel-Bulkley model (b) in dimensionless form. The Newtonian fluid is a standard fluid model for the lid-driven cavity problem. One can observe that due to the high viscosity in the non-Newtonian fluid there is no central vortex as in the Newtonian model.

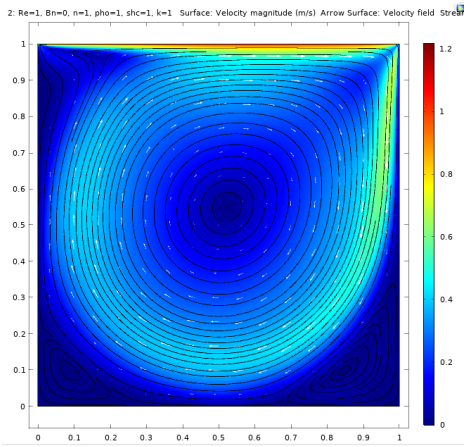

(a) The velocity field for the Newtonian model.

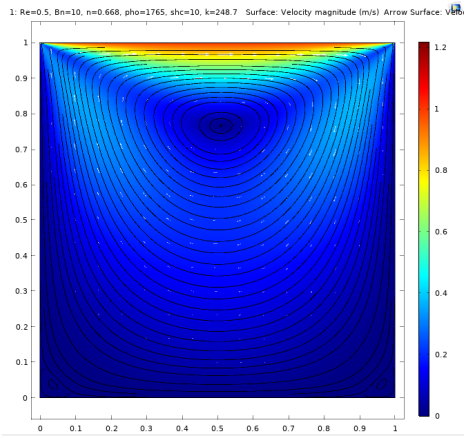

(b) The velocity field for the modified Herschel-Bulkley model.

Figure 4-8: Plots of velocity profiles for the Newtonian and modified Herschel-Bulkley models applied to the lid-driven cavity flow problem.

The line graphs presented in Fig. 4-9 describe the velocity profiles for the Newtonian (green line) and modified Herschel-Bulkley (blue line) models. Since in the Newtonian fluid model the viscosity is constant, the velocity varies greatly with sharp decline in the center of the cavity. In contrast to the Newtonian model, the velocity for the modified Herschel-Bulkley model does not exceed 0.2 m/s.

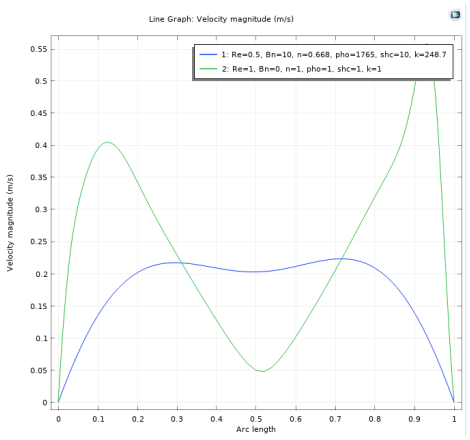

(a) The velocity along the horizontal line.

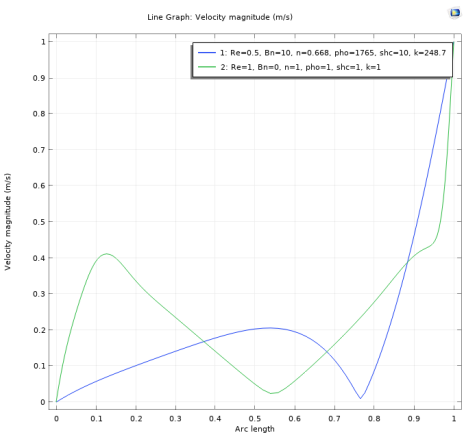

(b) The velocity along the vertical line.

Figure 4-9: Plots of velocity profiles for the modified Herschel-Bulkley and Newtonian models applied to the lid-driven cavity flow problem presented along the horizontal and vertical centerlines.

The pressure profiles are presented in Fig. 4-10. The difference between two models Newtonian (green line) and non-Newtonian (blue line)can be clearly noticed.

The pressure for the Newtonian fluid along the horizontal centerline has only small decrease in the middle of the square cavity. However, the pressure profile for the modified Herschel-Bulkley model has greater amplitude with small decline from the left side, a rapid growth up to 500 Pa and a slight drop to the right side. The graph shows that the pressure profiles for the non-Newtonian model significantly differ from those corresponding to the Newtonian flow model.

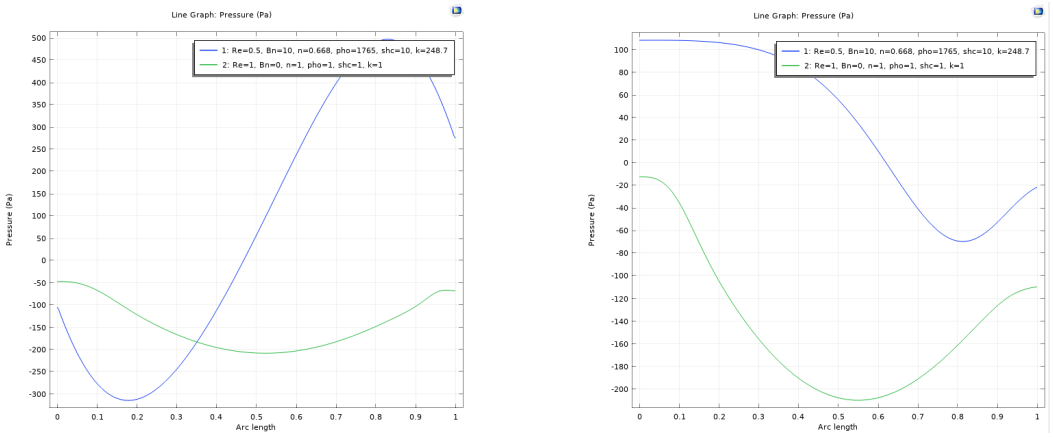

(a) The pressure along the horizontal line. (b) The pressure along the vertical line.

Figure 4-10: Plots of pressure profiles for the modified Herschel-Bulkley and Newtonian models applied to the lid-driven cavity flow problem presented along the horizontal and vertical centerlines.

4.5 Non-Newtonian fluid flow in cylindrical pipe

In this section we simulate the non-Newtonian flow based on the modified Herschel-Bulkley model in a cylindrical straight tube. The model is considered as steady-state, incompressible, laminar with no-slip at the wall. The tube die is a cylindrical pipe with radius 3 mm and height 24 mm. The viscosity of the fluid based on the modified Herschel-Bulkley model is considered in dimensionless form using the Bingham number.

Fig. 4-11 shows the velocity field and profile for the non-Newtonian fluid in a straight tube. It is clear that the velocity in the pipe smoothly decreases close to the boundary due to the no-slip condition, i.e. $\boldsymbol{v} = \mathbf{0}$ at the wall. For this kind of viscous fluid the maximum velocity is attained in the middle of the tube and it does

not exceed 0.1 m/s, see the velocity profile in Fig. 4-11(b).

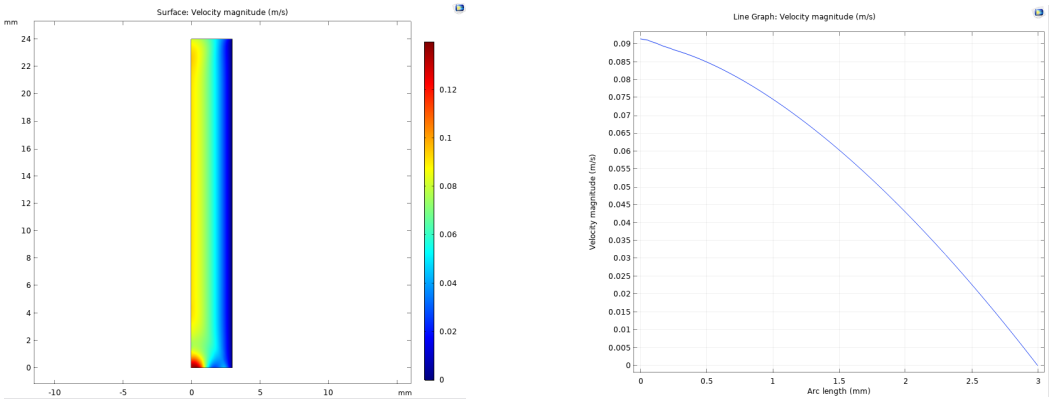

(a) The velocity field. (b) The velocity profile.

Figure 4-11: Plots of velocity field and profile for the modified Herschel-Bulkley model in the cylindrical pipe.

The pressure is slowly increasing from the bottom of tube upwards, see Fig. 4-12

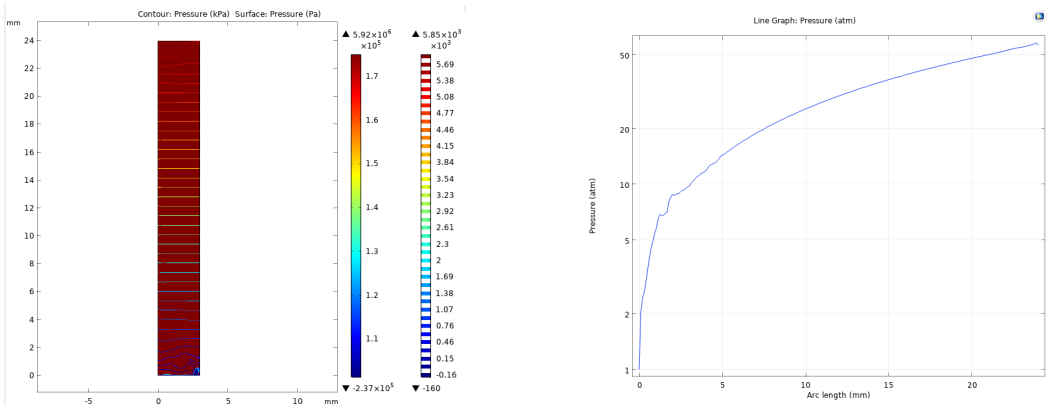

(a) The pressure field. (b) The pressure profile.

Figure 4-12: Plots of pressure field and profile for the modified Herschel-Bulkley model in the cylindrical pipe.

4.5.1 Pressure driven fluid flow in cylindrical pipe

Let us consider the Poiseuille fluid flow which is defined as steady-state, incompressible, laminar flow of viscous fluid between parallel plates divided by length h. The Poiseuille flow or pressure-driven flow occurs by pressure difference between inlet and outlet of the channel. Taking into account that the flow inside two parallel plates is

laminar, velocity can be determined in the following way

$$u = \frac{\Delta p(h^2 - r^2)}{2\mu L}$$

where Δp denote pressure difference, h is depth of the channel, r is the radius of the pipe, L is length of the tube, μ stands for the viscosity of the fluid. Using the above formula, we consider the Poiseuille flow with the parabolic inflow and no-slip at the wall. The pressure on the inlet is set to 1 atm and zero at the outlet. The graphs presented in Fig. 4-13 describe velocity distribution for the non-Newtonian fluid in the pressure driven flow. The viscous fluid flows smoothly with maximum velocity of 0.024 m/s at the center of tube and decreases at the no-slip wall.

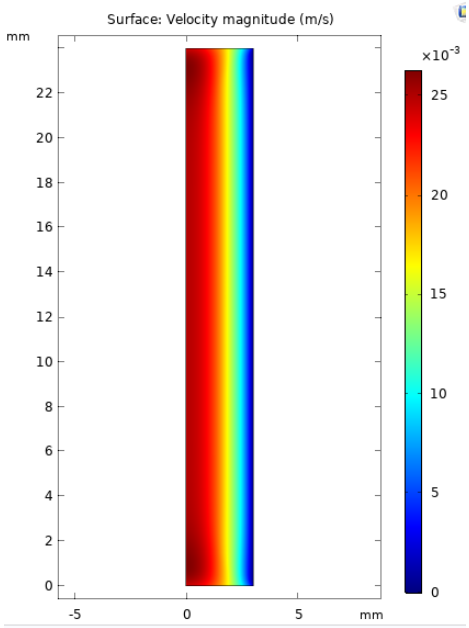

(a) The velocity field.

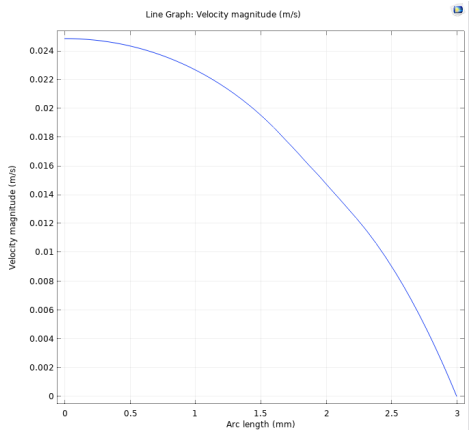

(b) The velocity profile.

Figure 4-13: Plots of velocity field and profile for the modified Herschel-Bulkley model in Poiseuille flow

Since there are no external additional forces, e.g., gravity, the fluid in the pipe moves due to the pressure difference between the inlet and outlet. The pressure profile for the modified Herschel-Bulkley fluid in the Poiseuille flow is presented in Fig. 4-14. The pressure slowly decreases down to the outflow. The pressure profile in Fig. 4-14(b) shows how the pressure changes along the symmetry line.

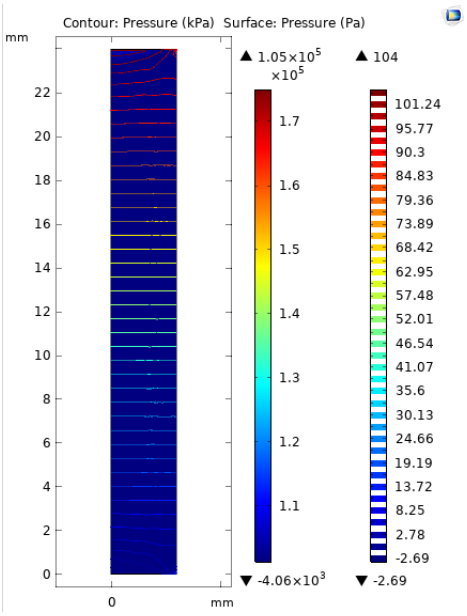

(a) The pressure field.

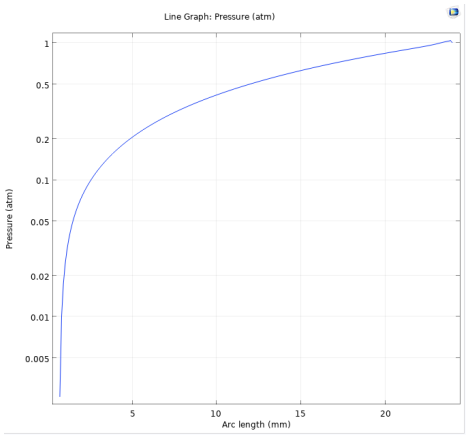

(b) The pressure profile.

Figure 4-14: Plots of pressure fields and profiles for the modified Herschel-Bulkley model in the Poiseuille flow.

4.5.2 Newtonian and non-Newtonian fluid in pressure driven pipe flow

In this section we will compare the Newtonian fluid flow model for the Poiseuille flow to the non-Newtonian one.

Fig. 4-15 shows the velocity profiles for the two different models. There is a significant difference between Newtonian and non-Newtonian flows. The maximum velocity of 0.16 in Fig. 4-15(a) appears in the middle of the tube. Then, the velocity gradually decreases to zero at the no-slip wall where $\boldsymbol{v} = \mathbf{0}$. However, the maximum velocity for the Herschel-Bulkley flow, see Fig. 4-15(b), does not exceed the value of 0.03 due to the high viscosity of the non-Newtonian fluid.

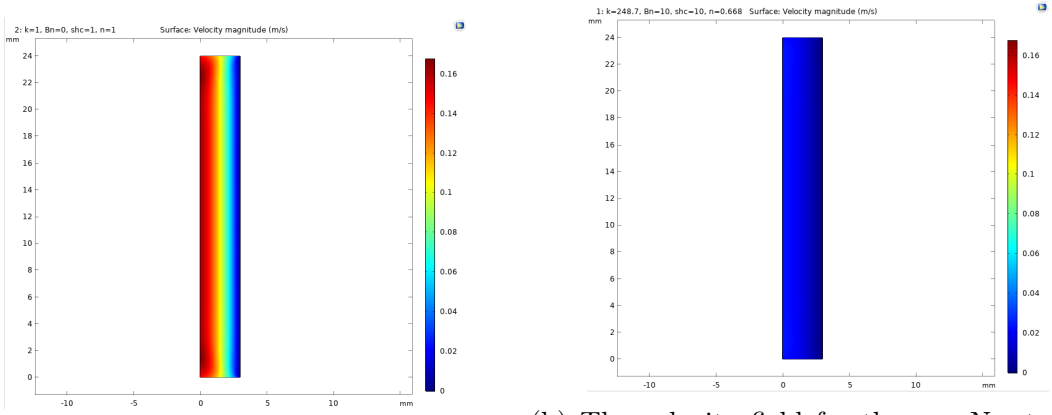

(a) The velocity field for the Newtonian flow. (b) The velocity field for the non-Newtonian flow.

Figure 4-15: The velocity fields for the Newtonian and modified Herschel-Bulkley Poiseuille pressure driven flows in the cylindrical pipe.

Fig. 4-16 shows the pressure fields for the Newtonian and non-Newtonian fluids in the Poiseuille flow. The distribution of the pressure in the two models is almost the same except the small oscillations close to the boundary in the non-Newtonian model. The maximum pressure slowly decreases up to zero at the outlet.

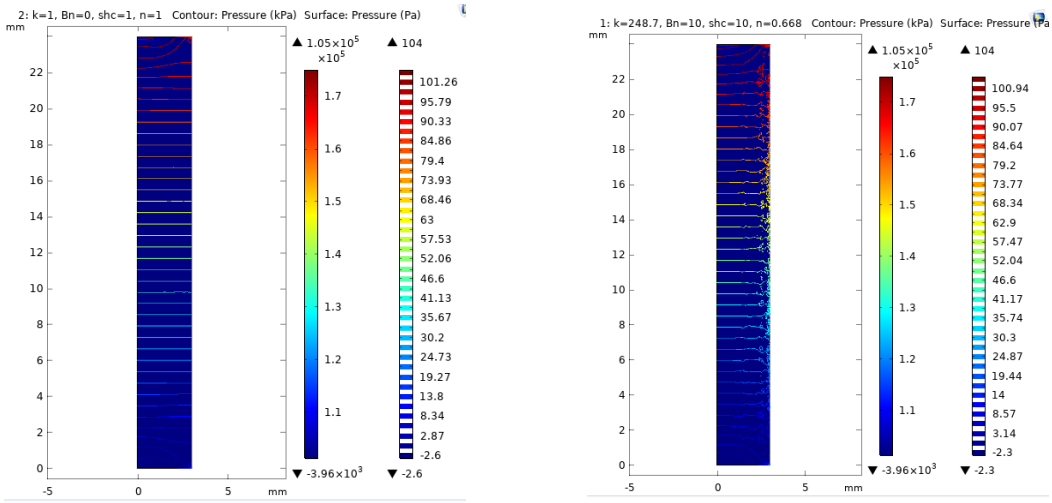

(a) The pressure field for the Newtonian Poiseuille flow. (b) The pressure field for the non-Newtonian Poiseuille flow.

Figure 4-16: The pressure fields for the Newtonian and modified Herschel-Bulkley models applied to the pressure driven Poiseuille flow in the cylindrical pipe.

The comparison between Newtonian and non-Newtonian models for the Poiseuille flow is presented in Fig. 4-17. The velocity profile for the Newtonian model (green

line) is much higher than the corresponding profile for the modified Herschel-Bulkley model (blue line). The plots of the velocity profiles confirm the fact that maximum velocity for the non-Newtonian model does not exceed 0.03, while the Newtonian fluid has approximately the maximum velocity 0.16. Fig. 4-17(b) shows the pressure profiles for the two models along the axis line. The pressure profiles almost overlap with each other. In other words, there is no much difference between pressure for the Newtonian and non-Newtonian Poiseuille flows in a cylindrical pipe.

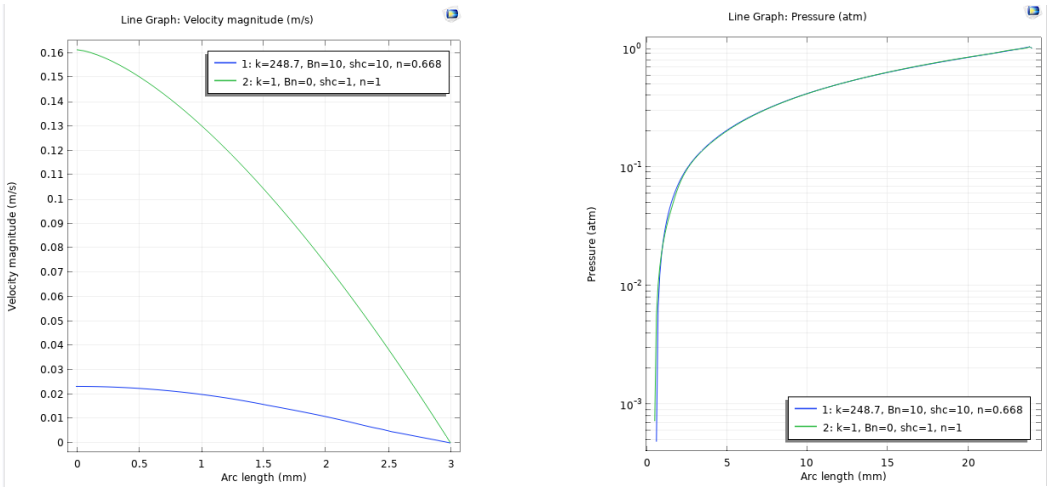

(a) The velocity profiles.

(b) The pressure profiles.

Figure 4-17: The velocity and pressure profiles for the Newtonian and modified Herschel-Bulkley Poiseuille pressure driven flows in a cylindrical pipe.

Chapter 5

Simulation results in COMSOL

After describing the rheology of ceramic paste, the next stage of our study are flow simulations for various geometries. The objective of this study is to visualize the velocity and pressure distribution of the flow over the domain. The Finite Element simulations for the flow of ceramic paste in the axis symmetric case were performed using the COMSOL Multiphysics and the non-Newtonian model. In this chapter results of simulations for the extrusion process of ceramic paste ram extruders of various geometrical forms will be presented.

5.1 Simulation results for extrusion dies of various geometries

5.1.1 Die Model 1

In the following we present simulation results for the ceramic paste extrusion in the case of three different extrusion die axis symmetrical geometries. The modeling and numerical approach for the ceramic paste extrusion has been presented in [2] for different geometries of the extrusion die where authors studied the effects of process parameters on the flow pressure and velocity.

The extrusion die from [2] consists of wide barrel with radius 10.0 mm which proceeds by right angle to the narrow part with radius 1 mm. The length of the

thin tube is 12.5 mm while the total die length is equal to 23.5 mm, see Fig. 5-1. In this study a triangular mesh was used to resolve the boundary layers at the walls of extrusion die [44]. The mesh consists of quite fine triangular cells in order to obtain the finite element solutions of high accuracy.

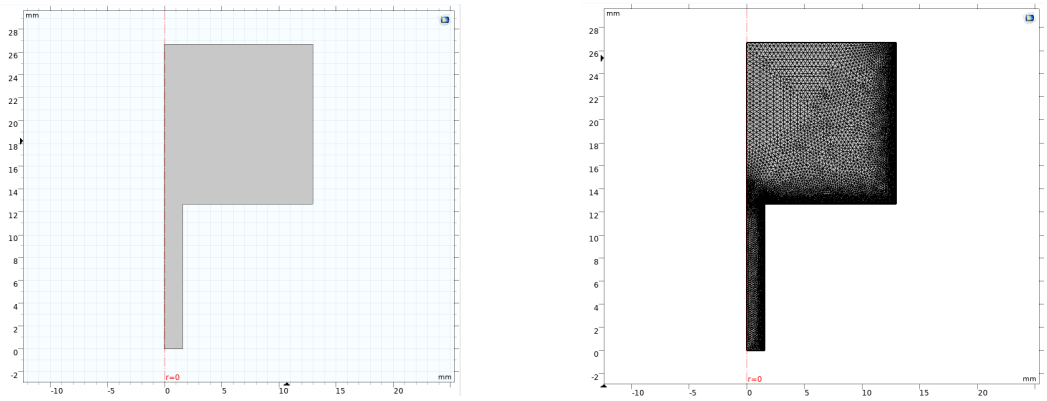

(a) The geometry of extrusion die.

(b) The mesh for the extrusion die.

Figure 5-1: The geometry for the first model of extrusion die (axis symmetry) and its mesh.

Herschel-Bulkley model

Let us analyze the extrusion process of ceramic paste using modified version of Herschel-Bulkley model in non-dimensional form. The experimental data of velocity are from [38] where the paste contains 50 volume %of alumina, 25 volume % of high density polyethylene, 23 volume % of paraffin wax and 2 volume % of stearic acid. The fitted parameters from [2] are presented in Table 5.1. The velocity fields

Parameter	Value
Critical shear rate, [1/s]	10.0
Yield stress, [Pa]	1103.0
Consistency index, [kg/m s]	248.7
Power-law index, [-]	0.668
Bingham number, [-]	10.0

Table 5.1: Parameters for the modified Herschel-Bulkley model.

for the Bingham plastics in extrusion die are presented in Fig. 5-2. Fig. 5-2 describes the velocity distribution in the main barrel. The velocity attains its maximum in the center region of die and slows down close to the boundary. Notice that in this die

geometry there is a region with zero velocity. The fluid does not move at the corner. The next graph shows velocity distribution in the narrow die. The fluid moves with high velocity in die and decreases at the wall due to the no-slip boundary conditions. The following plots shown in Fig. 5-3 represent the velocity profiles along the cut-line

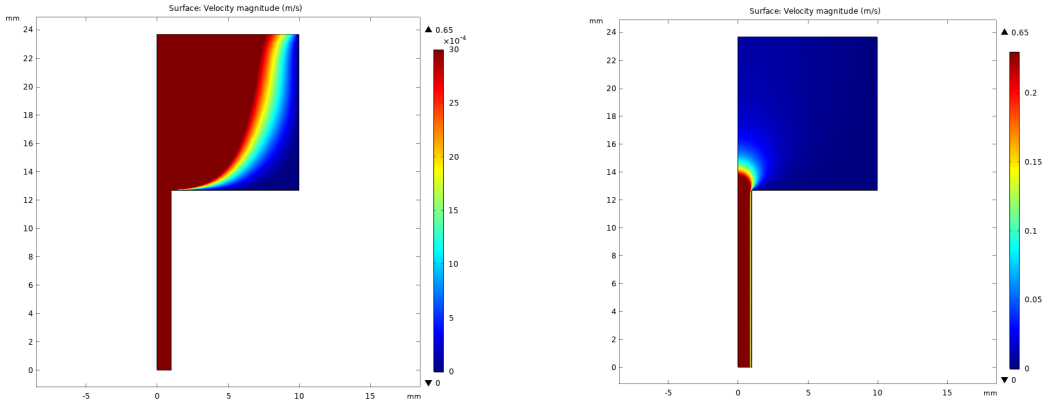

(a) The velocity field in the barrel. (b) The velocity field in the narrow die.

Figure 5-2: The velocity distributions in the ram extruder for the modified Herschel-Bulkley model.

at the center of wide barrel and the tube with a small radius. In the center of die fluid has velocity 0.16 m/s. Then it is rapidly decreasing such that in half arc length velocity of the fluid is 4 times less then maximum. Close to boundary of the die velocity is approaching to zero because of there is no slip on the wall. Plot (b) presents parabolic velocity profile in tube with smaller radius. Velocity of the fluid smoothly decreases to the die boundary. The COMSOL Multyphysics software computes the solution to

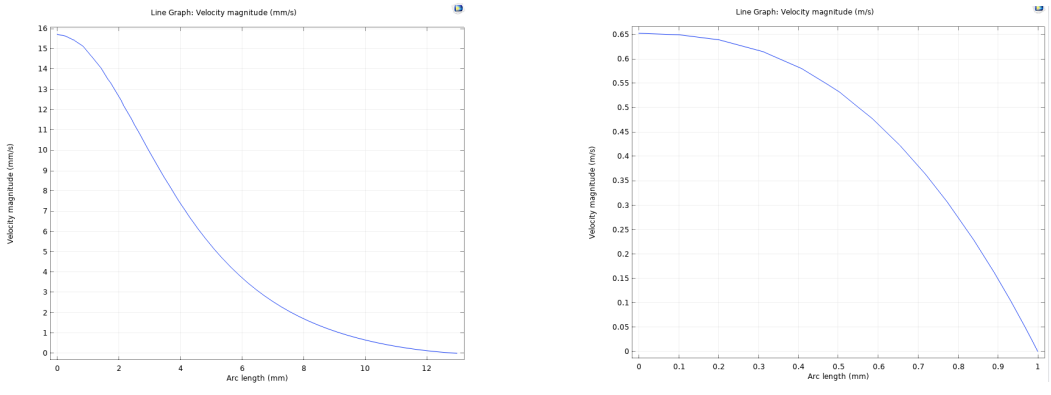

(a) The velocity profile in the barrel. (b) The velocity profile in the narrow die.

Figure 5-3: The velocity profiles in the ram extruder for the modified Herschel-Bulkley model.

the laminar flow problem for velocity components (v_r, v_θ, v_z) and the relative pressure

p. However, in this study, we have used boundary condition defined by the absolute pressure 1 atm at the outlet. The plot of pressure distribution in the extrusion die is presented in Fig. 5-4(a). The pressure is constant and of high magnitude in the wide barrel and decreases towards the outlet. The plot of the pressure profile presented in Fig. 5-4(b) confirms this finding. The pressure linearly increases in the thin tube and then remains maximal in a wide part of the extrusion die.

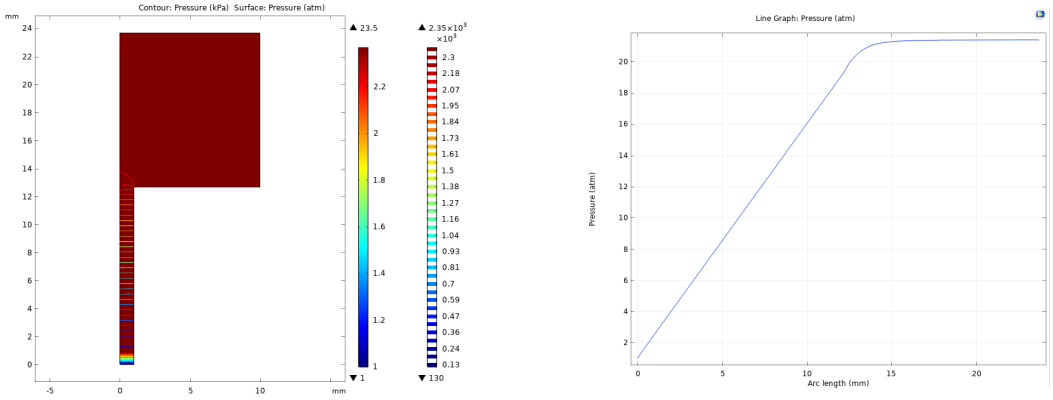

(a) The pressure field.

(b) The pressure profile.

Figure 5-4: The pressure distribution and profile in the ram extruder for the modified Herschel-Bulkley model.

Parameter study for Model 1

In order to study the extrusion process in Model 1 of die, the modified Herschel-Bulkley equations in the dimensionless form were used where a parameter, the so-called Bingham number was introduced. As in the case of lid-driven cavity flow problem, the auxiliary sweep was used to study velocity and pressure profiles for various Bingham numbers. The graphs in Fig. 5-5 show the velocity distribution in the extrusion die for the small and high values of Bingham number. The velocity fields do not differ significantly for various Bingham numbers. However, by inspecting 1D plots in Fig. 5-6 one can see more accurate the small changes of velocity when the Bingham number varies. The velocity in the main barrel declines strongly from the middle of die up to the wall. In general, the velocity profile in a wide and narrow parts of the die are similar to those from the previous study. Fig. 5-6(b) shows the usual velocity profile in the narrow tube where the velocity of the fluid

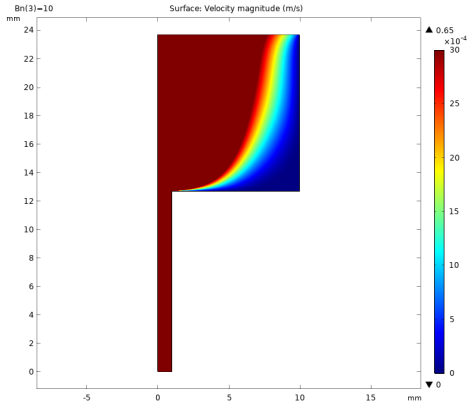

(a) The velocity field in the barrel for the Bingham number 10.

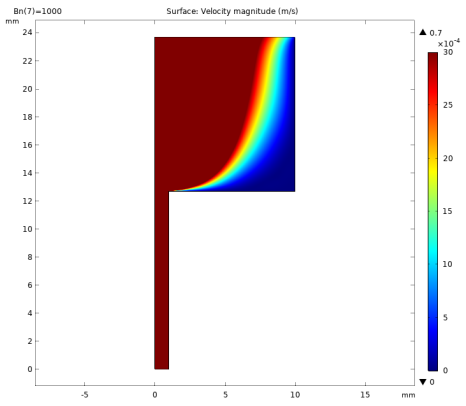

(b) The velocity field in the barrel for the Bingham number 1000.

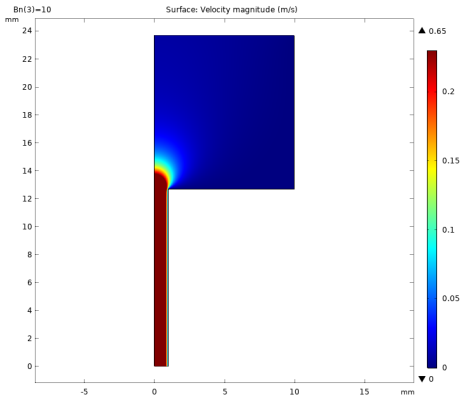

(c) The velocity field in the narrow die for the Bingham number 10.

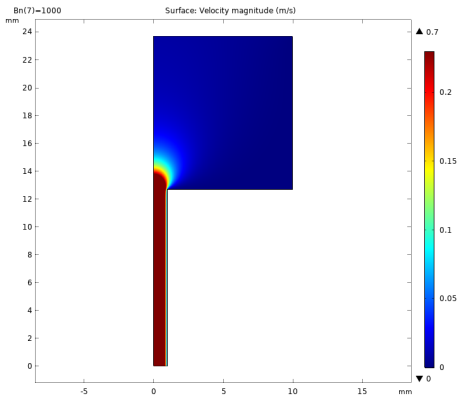

(d) The velocity field in the narrow die for the Bingham number 10

Figure 5-5: The velocity distributions in the extrusion die for the modified Herschel-Bulkley model and various values of Bingham number.

attains its maximum value in the middle and slowly decreases to zero due to the no-slip boundary condition. There is a small difference in the velocity in the central region of die for various Bingham numbers. All graphs show only minor changes of velocity when the Bingham number varies, i.e. changing the Bingham number does not have much influence on velocity distribution of alumina paste in the extrusion die. The pressure distribution for the modified Herschel-Bulkley model in the case of small and high value Bingham numbers is presented in Fig. 5-7. The color of contour lines defines the pressure of fluid in the extrusion die. There is a small difference between pressure distributions. However, 1D plots in Fig. 5-8 show the pressure more precisely for various Bingham numbers. Fig. 5-8 shows the pressure distribution along

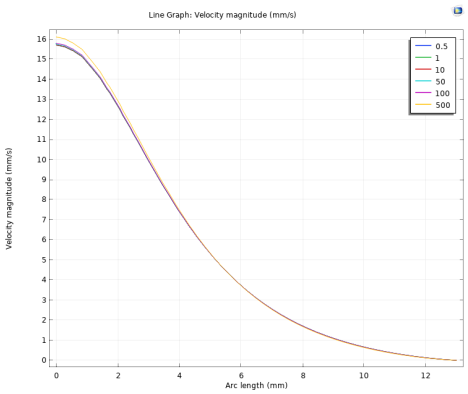

(a) The velocity profile in the barrel.

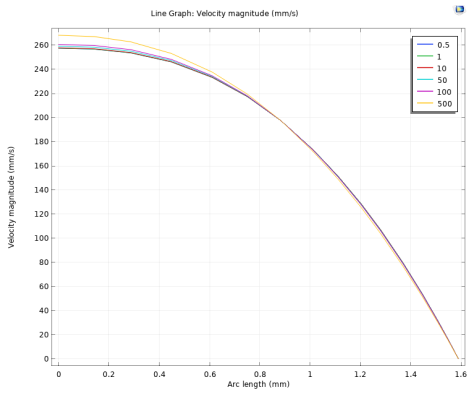

(b) The velocity profile in the narrow die.

Figure 5-6: The velocity profiles for various values of Bingham number.

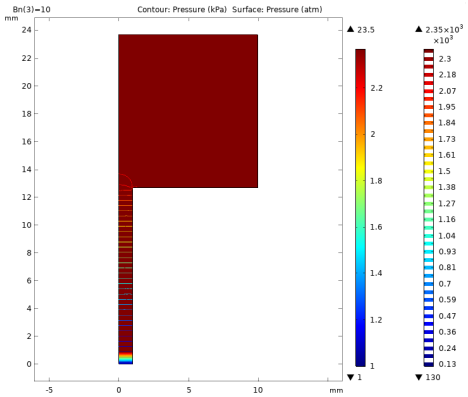

(a) The pressure field for the Bingham number 10.

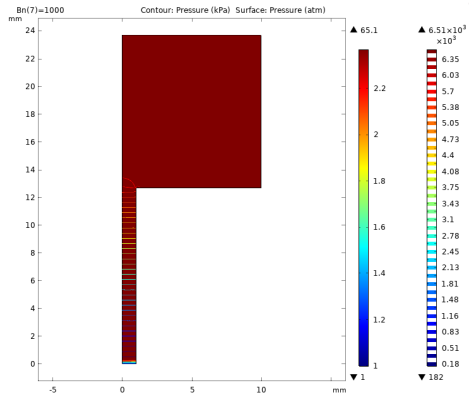

(b) The pressure field for the Bingham number 1000.

Figure 5-7: The pressure distributions for various values of Bingham number.

the symmetry line of the extrusion die. The pressure increases from the bottom up in the tube with a small die radius. The pressure remains constant in the main barrel. The pressure grows linearly in the narrow tube. Unlike the velocity profiles, there is a significant difference in the pressure when the Bingham number varies. As the Bingham number becomes larger, the pressure becomes higher. In other words, the Bingham number has significant effect on pressure of the ceramic paste in the extrusion die.

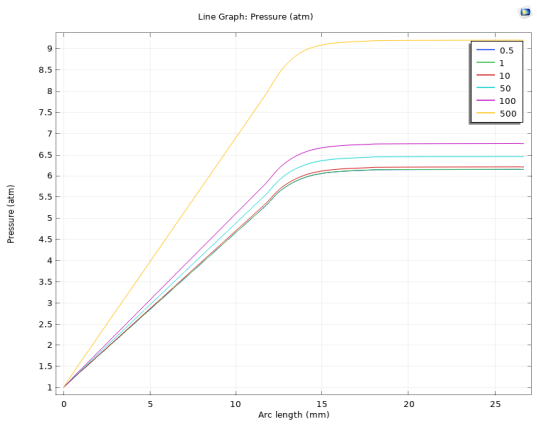

Figure 5-8: The pressure profiles for various Bingham numbers.

Newtonian and non-Newtonian fluid in extrusion die

The flow behaviour for the Newtonian and non-Newtonian fluids will be compared for the die Model 1. The comparison between these two viscous models will be provided. The non-Newtonian model is based on modified Herschel-Bulkley equations. The graphs in Fig. 5-9 show the velocity distributions of non-Newtonian and Newtonian fluids in the ram extruder die. The velocity attains its maximum in the middle of the tube and slows down close to the corner part of the barrel. There is no significant difference between plots of these two models which is also confirmed by velocity profiles presented in Fig. 5-11 . The pressure distribution in the extrusion die for the non-Newtonian and Newtonian fluids are shown in Fig. 5-10. Fig. 5-10(a) illustrates the maximum pressure that is attained at the corner between wide and narrow tube and slowly decreases down to the outlet of the die. The normal atmosphere pressure of 1 atm is set at the outlet. The graph in Fig. 5-10(b) shows the pressure distribution in the ram extruder for the Newtonian fluid. The green color of the surface in the main barrel indicates that the pressure does not exceed 1.7 atm and decreases down to the outlet, i.e. the pressure is gradually decreasing up to 1 atm. Comparing with the Newtonian fluid, we observe that the pressure of the ceramic paste in the extrusion die is significantly higher. The velocity profiles in the extrusion die for the Newtonian and non-Newtonian fluids are presented in Fig. 5-11. The velocity profiles are similar to those presented in the parameter study for various Bingham numbers.

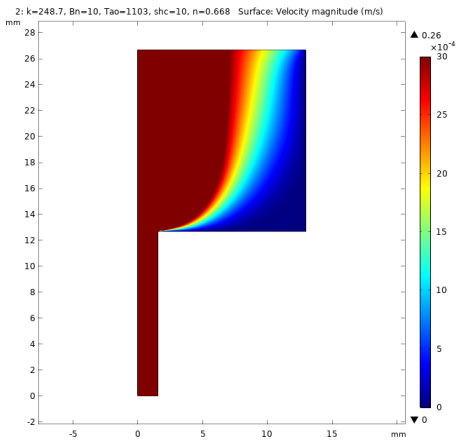

(a) The velocity field in the barrel for the non-Newtonian fluid.

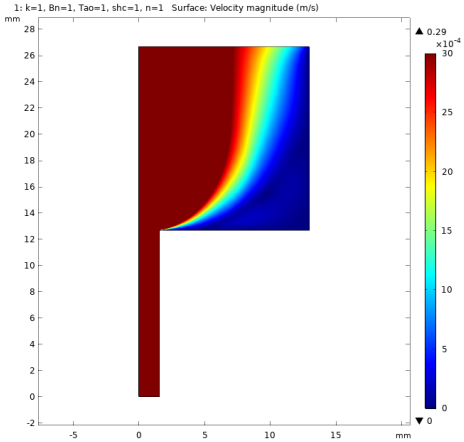

(b) The velocity field in the barrel for the Newtonian fluid.

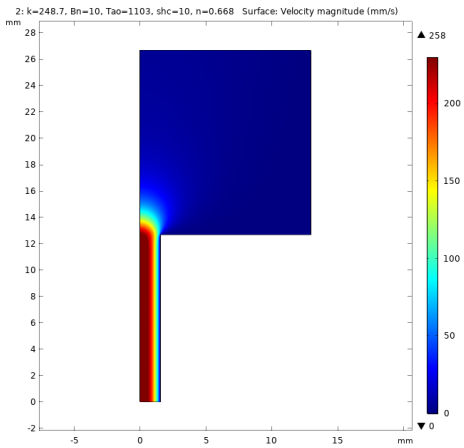

(c) The velocity field in the narrow die for the non-Newtonian fluid.

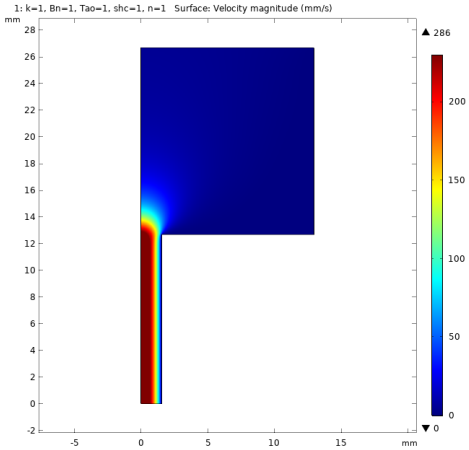

(d) The velocity field in the narrow die for the Newtonian fluid.

Figure 5-9: The velocity distributions in extrusion die for the non-Newtonian and Newtonian fluids.

Here, we compare the Newtonian (blue line) and non-Newtonian (green line) fluid flows. The maximum velocity for the Herschel-Bulkley model is lower than that one for the Newtonian model. However, the velocity for both cases are close and end up with zero at the boundary. The same observation can be done for the velocity in the narrow die. The maximum velocity for the Newtonian fluid is bigger than that one for the Herschel-Bulkley model. The profiles of parabolic shape are pretty close to each other such that the velocity in both cases slowly approaches zero at the die wall. We can conclude that the velocity distribution for Newtonian and non-Newtonian fluid flows do not differ significantly.

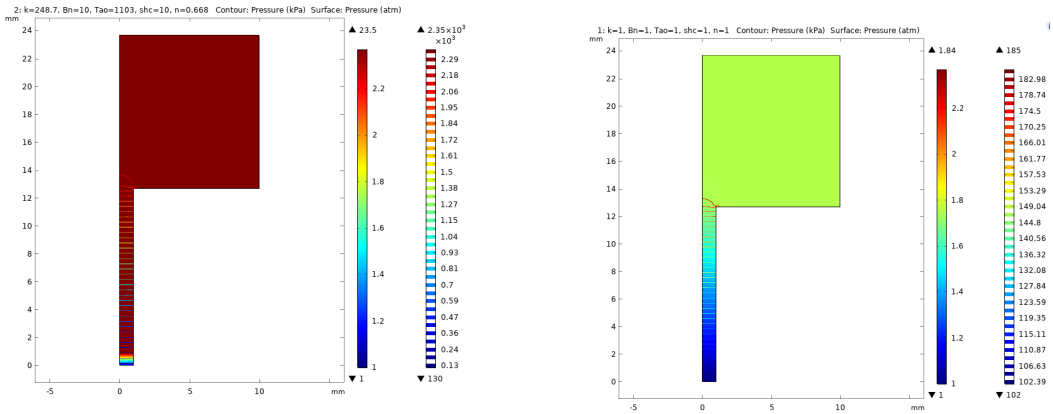

(a) The pressure field for the non-Newtonian fluid.

(b) The pressure field for the Newtonian fluid.

Figure 5-10: The pressure distributions in the ram extruder for the non-Newtonian and Newtonian fluids.

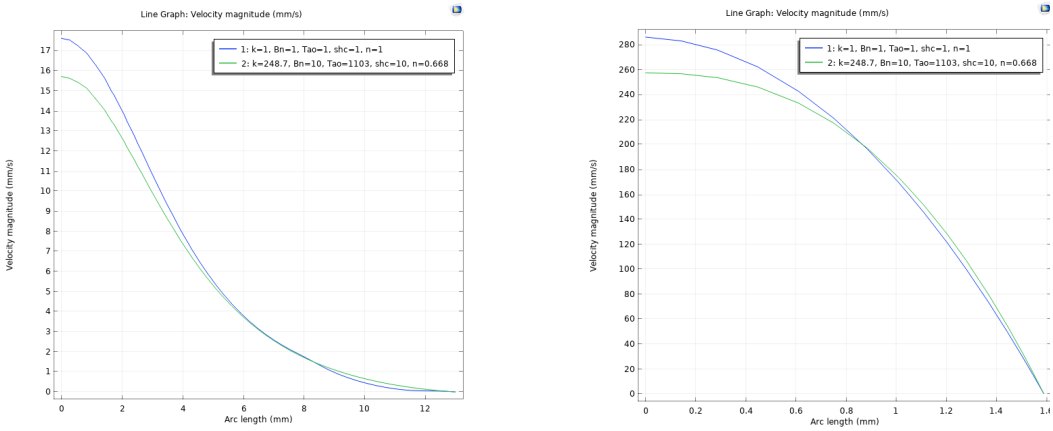

(a) The velocity profile in the barrel.

(b) The velocity profile in the narrow die.

Figure 5-11: The velocity profiles in the ram extruder for the non-Newtonian and Newtonian fluids.

5.1.2 Die Model 2

Now, we want to study the extrusion process for the ram extruder of slightly different form. The die has a skewed corner so that there is a transition part where the fluid can flow down to the thin tube more smoothly, see Fig. 5-12(a). In the axis symmetrical case the extrusion die consists of the barrel with the wide radius of 10 mm and height of 11 mm. There is a thin tube with radius of 1 mm and length of 9.5 mm. The right corner has been skewed in order to get smooth transition between the barrel side and the narrow die. The triangular mesh with fine cells, see Fig. 5-12(b), was applied in the following simulations.

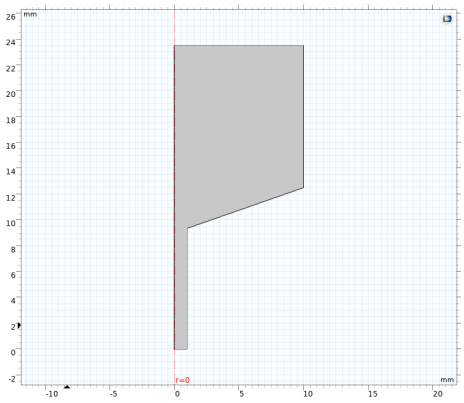

(a) The geometry of the extrusion die.

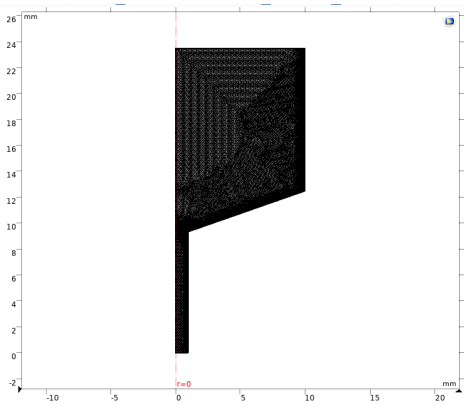

(b) The mesh for the extrusion die.

Figure 5-12: The geometry for the second model of extrusion die (axis symmetry) and its mesh.

Herschel-Bulkley model in extrusion die

The simulations for the ceramic paste extrusion process were performed using the CFD module of the COMSOL Multyphysics. The regularized Herschel-Bulkley model with the same parameters for the alumina paste as for the *Die Model 1* was applied. All input parameters and boundary conditions are the same as in *Die Model 1*, i.e. this is an incompressible, steady-state, laminar flow with no-slip at the wall and the normal atmosphere pressure at the outlet. The velocity fields for the modified Herschel-Bulkley model are presented in Fig. 5-13. Fig. 5-13(a) shows the velocity of the fluid in the main barrel. The fluid with high velocity flows down to the thin tube, the velocity decreases close to the boundary side. In contrast with *Die Model 1* the zero velocity region is much smaller at the corner. This means that less amount of paste significantly slows down at the corner. The paste flows more smoothly due to the skewed corner. Fig. 5-13(b) shows the velocity field in the narrow die. The velocity of the fluid is higher in the center of tube and decreases at the die walls. Fig. 5-13(c) is a 3D plot of the velocity distribution in the narrow die using the axis symmetry of the extruder. The velocity profiles of the ceramic paste in the extrusion die are presented in Fig. 5-14. The first graph in Fig. 5-14 describes the velocity profile through the center of the wide barrel in the horizontal direction. The maximum velocity of the fluid is attained in the middle of the die and it is about 0.014 m/s. Then, the velocity slowly decreases up to the boundary. Unlike the *Die*

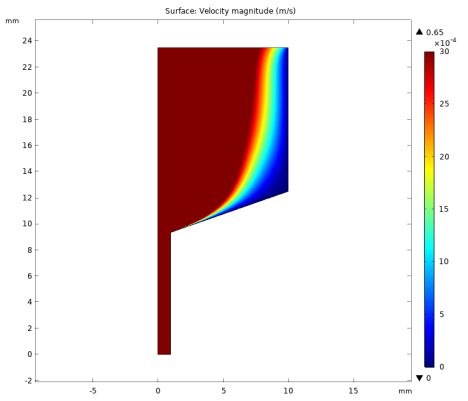

(a) The velocity field in the barrel.

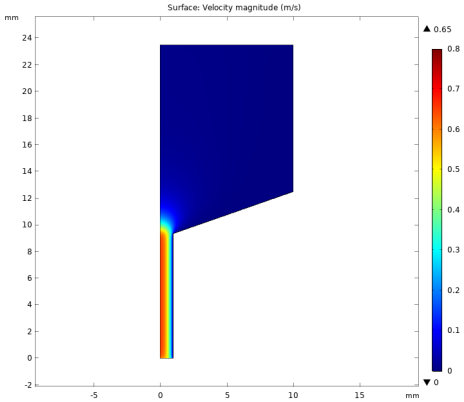

(b) The velocity field in the narrow tube.

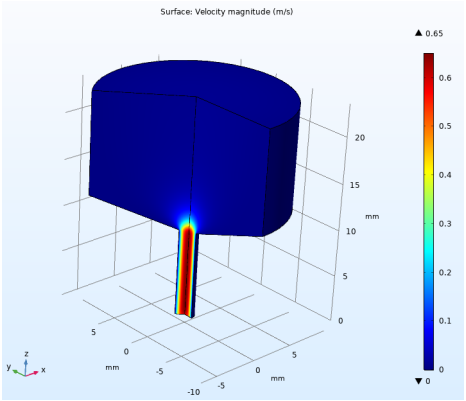

(c) 3D plot of the velocity field.

Figure 5-13: The velocity field in the ram extruder for the modified Herschel-Bulkley model.

Model 1, the fluid velocity in this form of die gradually declines to zero. The plot of velocity profile in the narrow die is similar to the graph of *Die Model 1*. The velocity profile has a parabolic shape with maximum value 0.65 m/s attained in the middle of the narrow tube. The pressure in the extrusion die is illustrated in Fig. 5-15. The color of the surface in Fig. 5-15(a) indicates that the pressure is constant and of high value in the wide part of the die. Then, it decreases towards the outlet where the pressure is set to 1 atm. The pressure profile presented in Fig. 5-15(b) is determined along the symmetry line. It shows that the pressure slowly increases in the thin tube from the outlet to the barrel side. The pressure curve goes up with a small rounding. Concluding, the pressure in *Die Model 2* changes more smoothly than in *Die Model 1* due to the skewed corner.

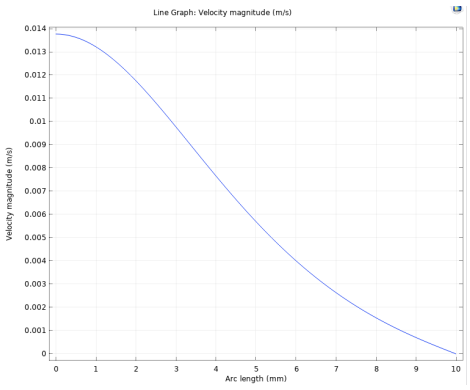

(a) The velocity profile in the barrel.

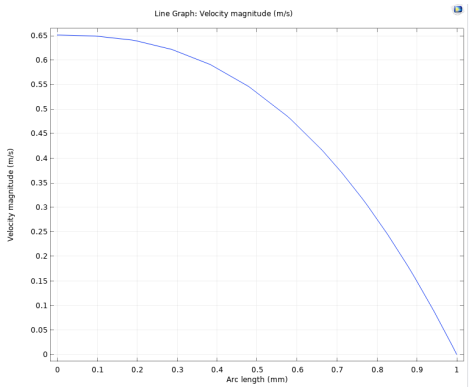

(b) The velocity profile in the narrow tube.

Figure 5-14: The velocity profiles in the ram extruder for the modified Herschel-Bulkley model.

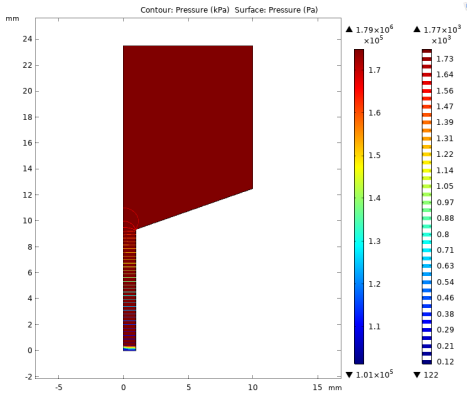

(a) The pressure field.

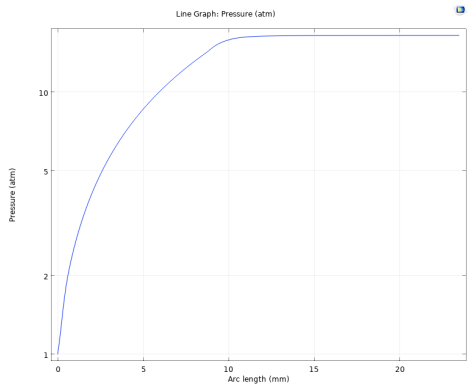

(b) The pressure profile.

Figure 5-15: The pressure distribution and profile in the ram extruder for the modified Herschel-Bulkley model.

Parameter study of modified Herschel-Bulkley model in extrusion die Model 2

In this part, the velocity and pressure distributions for the regularized Herschel-Bulkley model will be studied for various values of the Bingham number. Fig. 5-16 shows the velocity distribution of the fluid in the extrusion *Die Model 2*. The velocity profiles in the barrel part are shown for low and high Bingham numbers. One can observe only a minor change of the fluid velocity when the Bingham number varies. However, 2D plots do not precisely show the differences.

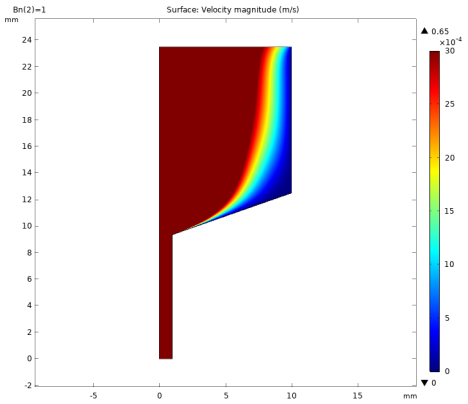

(a) The velocity field in the barrel for the Bingham number 1.

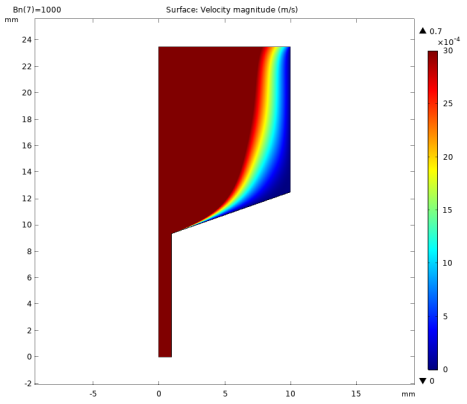

(b) The velocity field in the barrel for the Bingham number 1000.

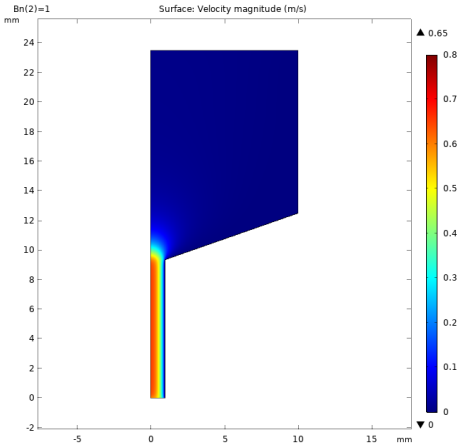

(c) The velocity field in the narrow tube for the Bingham number 1.

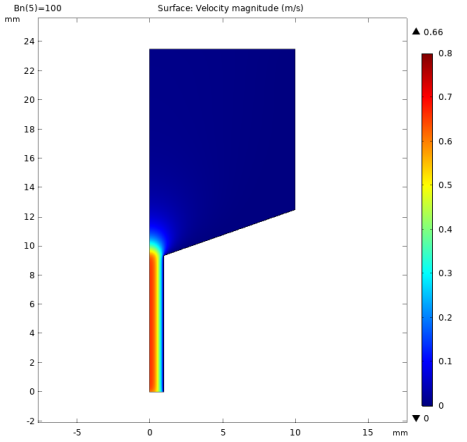

(d) The velocity field in the barrel for the Bingham number 100.

Figure 5-16: The velocity distribution in the ram extruder for the modified Herschel-Bulkley model and various values of Bingham number.

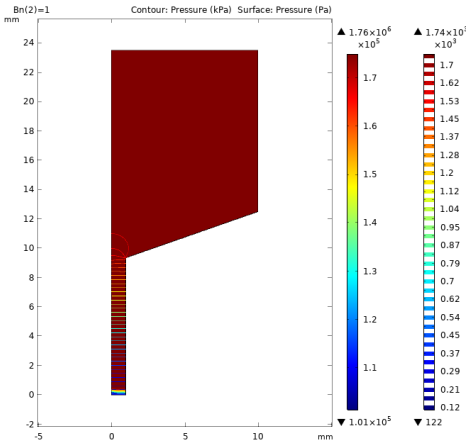

(a) The pressure field for the Bingham number 1.

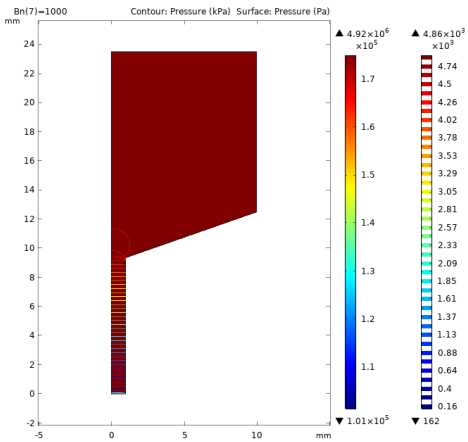

(b) The pressure field for the Bingham number 1000.

Figure 5-18: The pressure distribution in the extrusion die for the modified Herschel-Bulkley model and various values of Bingham number.

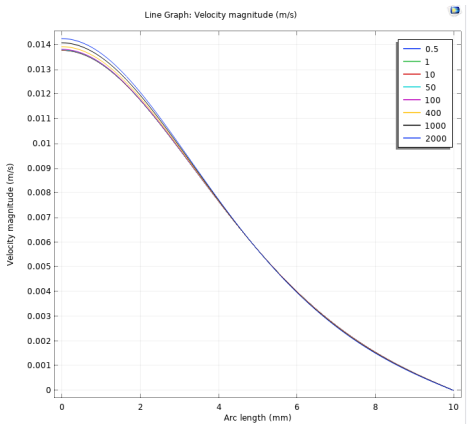

(a) The velocity profiles in the barrel.

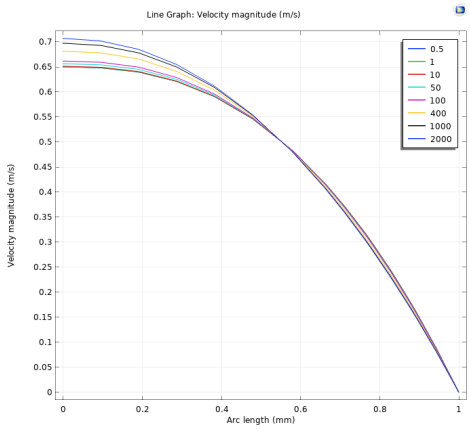

(b) The velocity profiles in the narrow tube.

Figure 5-17: The velocity profiles in the ram extruder for the modified Herschel-Bulkley model and various values of Bingham number.

The graphs in Fig. 5-17 show the velocity profiles in the extrusion *Die Model 2* for the modified Herschel-Bulkley model and various values of Bingham number, $Bn = 0.5, 1, 10, 50, 100, 400, 1000, 2000$.

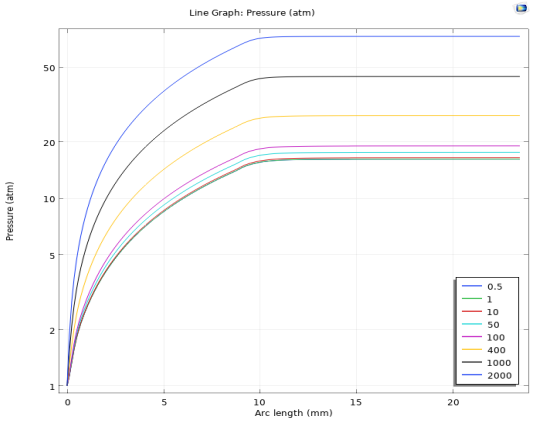

Figure 5-19: The pressure profiles for the modified Herschel-Bulkley model and various values of Bingham number.

The velocity profiles are of the same shape as in the previous model. There is only a small difference in the maximum of velocity for each case. The profiles almost coincide with each other. Clearly, changing the Bingham number in viscosity of the fluid does not have a significant effect on the velocity profile. The pressure distributions in the extrusion die are presented in Fig. 5-18 for low and high Bingham numbers. There is a slight difference between the graphs for the pressure. In Fig. 5-19

the pressure profiles in the extrusion *die Model 2* are presented for various Bingham numbers. In general, the pressure curves are of the same shape as the pressure profiles in the previous model. We observe that as the Bingham number increases the pressure magnitude grows. Concluding, we state that the pressure in the extrusion die is directly proportional to the Bingham number.

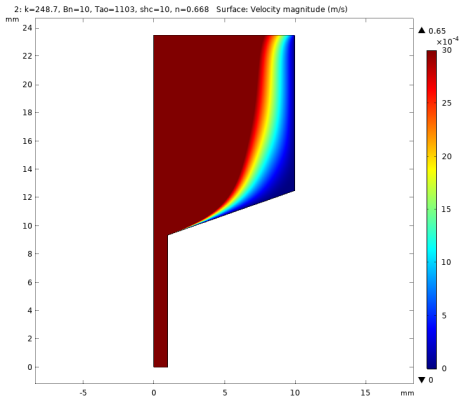

(a) The velocity field in the barrel for the non-Newtonian fluid.

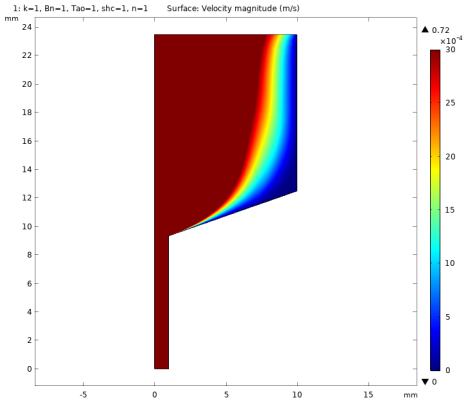

(b) The velocity field in the barrel for the Newtonian fluid.

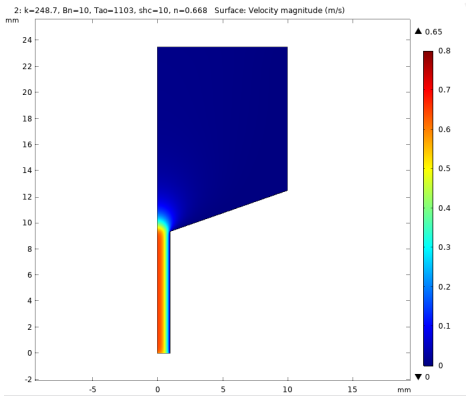

(c) The velocity field in the narrow tube for the non-Newtonian fluid.

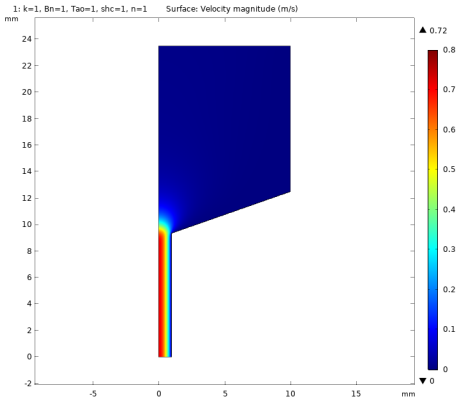

(d) The velocity field in the narrow tube for the Newtonian fluid.

Figure 5-20: The velocity distributions in the ram extruder for the non-Newtonian and Newtonian fluids.

Newtonian and non-Newtonian fluids in extrusion die

Now, we compare the velocity and pressure distributions for the Newtonian and non-Newtonian fluids in *Die Model 2*.

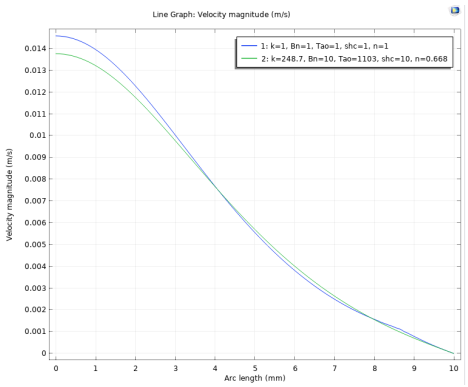

(a) The velocity profile in the barrel.

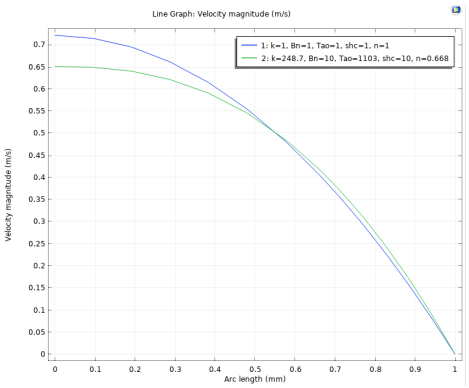

(b) The velocity profile in the narrow tube.

Figure 5-21: The velocity profiles in the ram extruder for the non-Newtonian and Newtonian fluids.

The velocity distributions for the non-Newtonian and Newtonian fluids are presented in Fig. 5-20. At the first glance, the graphs are the same. The velocity for the Newtonian fluid is greater in the narrow die than in the center of the die. This fact can be confirmed by inspecting 1D plots for the velocity profiles in Fig. 5-21. The

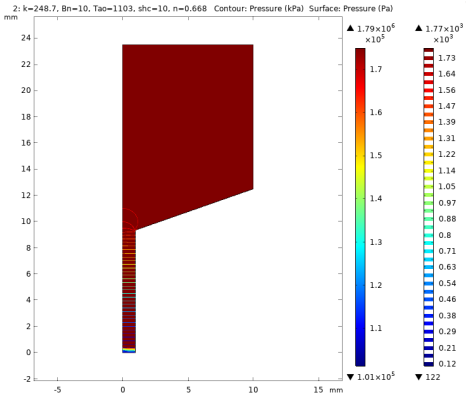

(a) pressure of non-Newtonian fluid

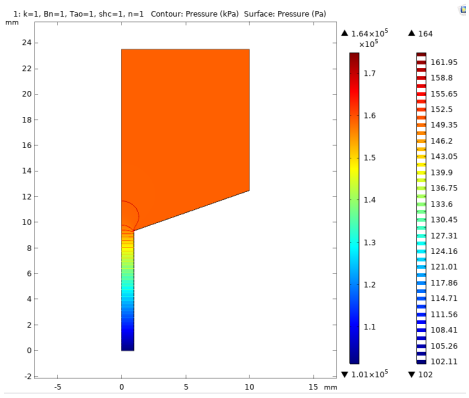

(b) pressure of Newtonian fluid

Figure 5-22: Pressure distribution of non-Newtonian and Newtonian fluid in extrusion die

velocity profiles for the Newtonian and non-Newtonian fluids show that the curve for the Newtonian (blue line) and non-Newtonian (green line) fluids are extremely close to each other.

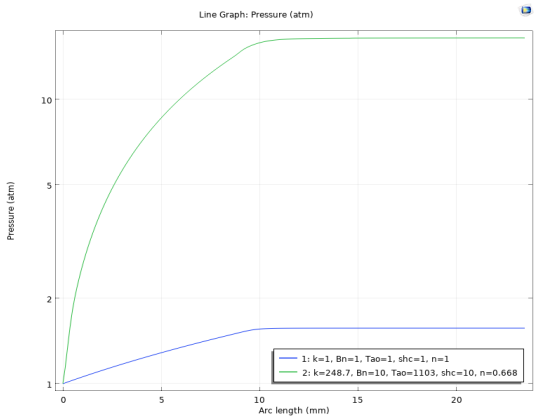

Figure 5-23: Pressure profile of Newtonian and non-Newtonian fluid in extrusion die

There is a minor difference in the maximum velocity. The curves for the modified Herschel-Bulkley model decrease more gradually than those for the Newtonian fluids. The same can be observed for the velocity profiles in the thin tube. The velocity curve for the Newtonian fluid has greater maximum than the velocity for the non-Newtonian fluid. The lines overlap each other in the decreasing direction, see Fig. 5-21. In Fig. 5-22 the pressure distributions for the non-Newtonian and Newtonian fluids are presented. There is a significant difference between the pressure profiles for the two fluid models. While the non-Newtonian fluid moves with maximum pressure 17 atm in the wide part of the die, the pressure of Newtonian fluid does not exceed 15 atm and slowly decreases in the die with smaller diameter. In other words, the pressure of Newtonian fluids in the extrusion die with skewed corner is much lower in the barrel side. Fig. 5-23 shows that the pressure magnitude for the non-Newtonian fluid (green line) is much greater than the pressure magnitude for the Newtonian model (blue line). The difference between two models is almost 10 atm. The pressure for the Newtonian fluid is linearly increasing up to 1.7 atm and stays at that level in the wide barrel. We notice that there is a significant difference between pressures in two types of fluids in the extrusion *Die Model 2*.

Computed viscosity

Ceramic pastes are fluid-particle suspensions whose flow behaviour depends on the viscosity function of the fluid, the solid-liquid ratio, the size of the particle and the

particle shape.

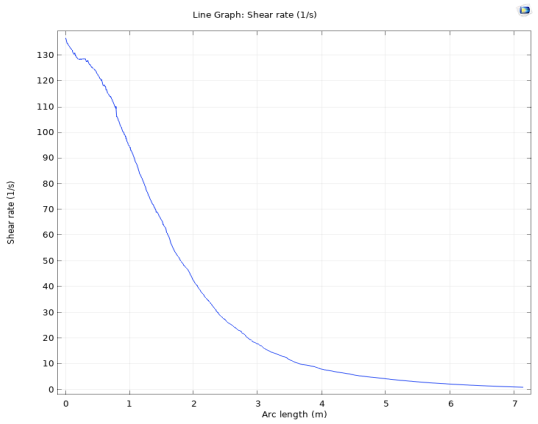

Figure 5-24: The computed viscosity of alumina paste for the modified Herschel-Bulkley model.

The recent studies show that at the high shear stress the shear stress function is basically determined by the shear rate function of the suspending fluid which means that the flow behaviour of the suspension is determined by the hydrodynamic forces within the particles. The modeling and qualitative analysis of ceramic paste extrusion are highly important in order to design and optimize the extrusion process for producing the high-value extrudates of required strength, form and morphology [45]. The computed viscosity of alumina paste is presented in Fig. 5-24. The graph was plotted in the transition region from the wide to the narrow channel. The curve of the shear rate starts from its maximum value 130 1/s and smoothly decreases till its minimum value.

5.1.3 Die Model 3

We will improve our simulation results by changing the geometry of the die. Using the form of *Die Model 2* we will build a new die geometry with rounded corners such that the viscous fluid will flow more smoothly into the narrow tube, see Fig. 5-25.

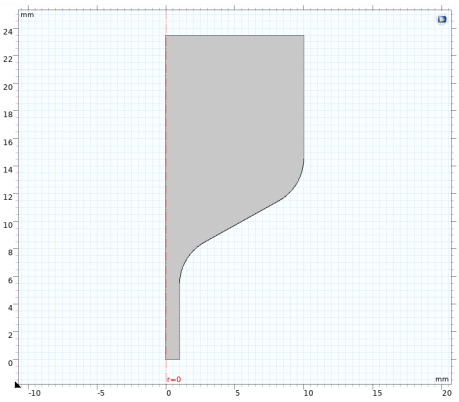

Figure 5-25: The Geometry of the extrusion *Die Model 3*.

The size of the extrusion die in *Die Model 3* is similar to *Die Model 2*. The extrusion die is axis symmetric and consists of the barrel with wide radius 10 mm and height 11 mm. The thin tube has radius 1 mm and length 9.5 mm. The right corner was skewed in order to achieve the more smooth transition between the barrel side and narrow tube. The corners of this transition part were rounded such that the non-Newtonian fluid will flow more smoothly.

Modified Herschel-Bulkley model

The extrusion process of ceramic paste is studied using the regularized version of Herschel-Bulkley model in the dimensionless form. This model is analyzed by the laminar flow module in COMSOL Multyphysics for incompressible, steady-state fluid flow. The initial and boundary conditions are the same as in *Die Model 1, 2*. There is no-slip at the die wall, the initial velocity is zero and the pressure is set to 1 atm at the die outlet. The parameters for the Herschel-Bulkley viscosity are chosen from Table 5.1.

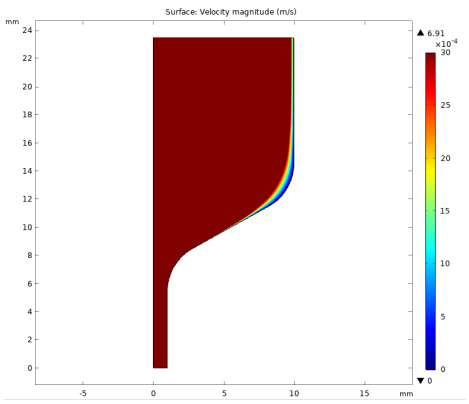

(a) The velocity field in the barrel.

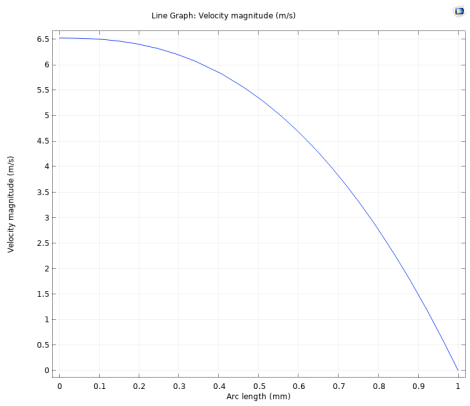

(b) The velocity profile in the narrow tube.

Figure 5-26: The velocity distribution in the barrel and the velocity profile in the narrow tube for the modified Herschel-Bulkley model.

Fig. 5-27 presents the velocity field and profiles for the regularized Herschel-Bulkley model in the new form of the extrusion die. In this case, we observe that the viscous fluid flows with maximum velocity in whole domain. There are no zero velocity regions where paste does not move. The fluid slows down close to the die walls due the no-slip condition. Similarly, the velocity in the narrow die is pretty high in the die center. The 3D plot in Fig. 5-27(c) shows the general view of the velocity in the ram extruder.

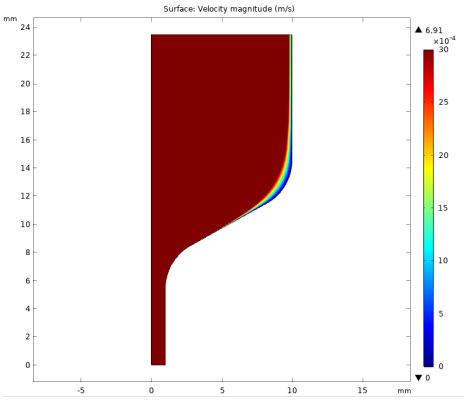

(a) The velocity field in the barrel.

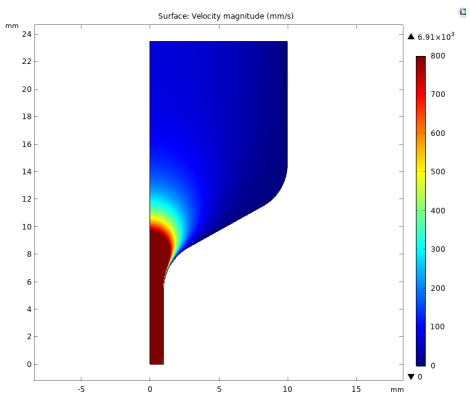

(b) The velocity field in the narrow tube.

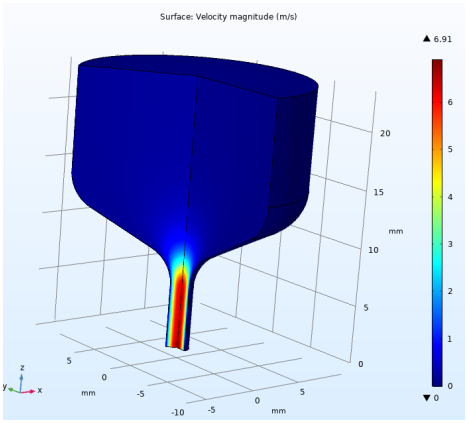

(c) 3D plot of the velocity field in the narrow tube.

Figure 5-27: The velocity distribution in the extrusion die for the modified Herschel-Bulkley model.

Finally, we present in Fig. 5-28 the velocity profiles for three die models studied in this chapter. It is clear from the graph velocity profile of *Model 1* is higher then profile of *Model 2*. However velocity of the paste in extrusion die with rounded corners is much greater, then other models. The pressure profiles of *Model 1* and *Model 2* are linearly increasing till 20 atm and 17 atm respectively, as it was shown in previous sections. Pressure profile of *Model 3* is much greater then profiles of two other models. In other words velocity and pressure profiles of extrusion die *Model 3* are noticeably higher then *Model 1* and *Model 2*.

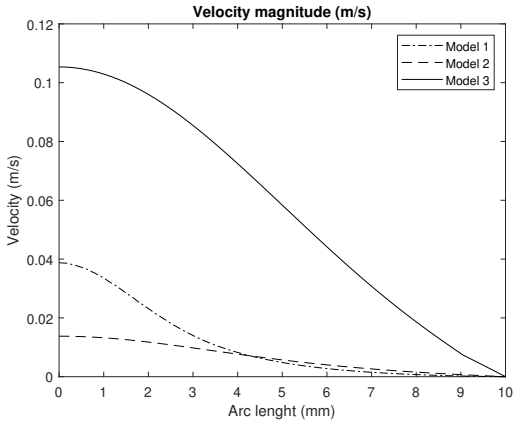

(a) The velocity profiles.

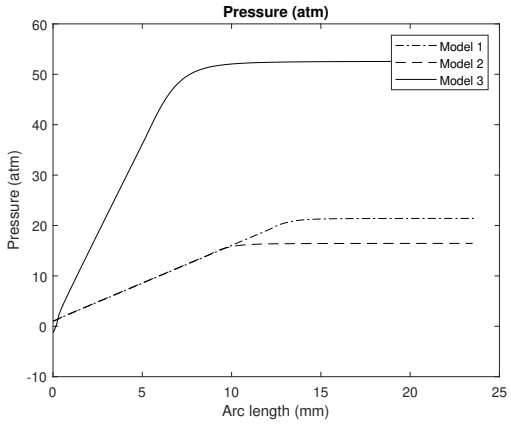

(b) The pressure profiles.

Figure 5-28: The velocity and pressure profiles in three types of the extrusion die models for the modified Herschel-Bulkley flow.

The die geometry and the form of the transition region has significant influence on the shape of the velocity and pressure profiles of ceramic paste extrusion in 3D printing.

Chapter 6

Conclusions

In this work, the mathematical model for the extrusion of ceramic paste with applications for 3D printing was established and numerically solved using the Finite Element software COMSOL. The mathematical model of the ram extrusion was defined using the continuity and momentum equations which were then numerically solved for the case of non-Newtonian fluids based on the modified Herschel-Bulkley equations. The concept of non-Newtonian fluids was presented in Chapter 2 where the special case of the Bingham model, i.e. modified Herschel-Bulkley model, was discussed. The governing equations for the model were presented as generalized axis symmetric, incompressible, laminar, steady-state Navier-Stokes equations. The finite element software COMSOL Multiphysics has been used to simulate the flow velocity and pressure distributions inside the extrusion die. The results of simulations were illustrated using 1D, 2D and 3D plots. Particularly, it was demonstrated that due to properties of the viscous fluid the velocity reaches its maximum value at the centre of the extrusion die and decreases close to the die boundaries. The viscosity of alumina paste was also approximated numerically and presented in the transition region. The line graph which represents the shear rate of the ceramic paste shows the gradual decline of the shear rate value in the extrusion die. Similarly, the results of the simulations show that the pressure of the fluid inside the extrusion die is constant and of high magnitude in the barrel part and it slowly decreases as the fluid moves to outlet in the narrow die. The die geometry has influence on the the shape of the

pressure profiles. The skewed corner in the transition region can reduce the pressure gradient. The obtained results can be useful to design and optimize the ceramic paste extruders.

Bibliography

[1] Li, M., L. Tang, R.G. Landers, and M.C. Leu, *Extrusion process modeling for aqueous-based ceramic pastes-Part 1: Constitutive model.* J. Manuf. Sci. Eng., 135:051008, 1-7 (2013a)

[2] B. Golman, P. Skrzypacz, W. Julklang, *Modeling and Numerical Study of Ceramic Paste Extrusion.* accepted for publication in Proceedings of APCChE 2019.

[3] Majić Renjo, Marijana, et al. *Rheological properties of aqueous alumina suspensions*, Materialwissenschaft und Werkstofftechnik 43.11 (2012): 979-983.

[4] Z. Chen, Z. Li, J. Li, C. Liu, C. Lao, Y. Fu, C. Liu, Y. Li, P. Wang, and Y. He, *3D printing of ceramics: A review.* J. Eur. Ceram. Soc., 39, 661-687 (2019)

[5] L.D. Landau and E.M. Lifshitz, *Fluid mechanics*, 1959

[6] A. Björn, P. Segura de La Monja, A. Karlsson, J. Ejlertsson, and Bo H. Svensson, *Rheological Characterization*, 2012

[7] I. Seyssiecq, J.H. Ferasse, and N. Roche, *State-of-the-art: rheological characterization of waste water treatment sludge.* Biochem Engin Jour, 2003, Vol.16, pp. 41-5.

[8] S.M. Chen, W.A. Bullogh and J. Hart. *CFD study of the flow in a radial clutch with a real electrorheological fluid.* Proc. of 11th Conference on Electrorheological Fluids and Magnetorheo-logical Suspensions, Journal of Physics: Conference Series 149 (2009)

[9] A. Hirn, *Finite element approximation of singular power-law systems*, Math. Comp., 82 (2013),pp.1247-68.

[10] K. Sverdrup, N. Nikiforakis, A. Almgren, *Highly parallelisable simulations of time-dependent viscoplastic fluid flow with structured adaptive mesh refinement.* Physics of Fluids 30.9 (2018): 093102.

[11] J. Málek. *Introduction to non-Newtonian fluid mechanics*, October (2012)

[12] W. Ostwald, *Über die Geschwindigkeitsfunktion der Viskosität disperser Systeme.* I. Colloid Polym. Sci., 36:99–117, 1925.

[13] A. de Waele, *Viscometry and plastometry.* J. Oil Colour Chem. Assoc., 6:33–69, 1923.

[14] P. J. Carreau, *Rheological equations from molecular network theories.* J. Rheol., 16(1):99–127, 1972.

[15] K. Yasuda, *Investigation of the analogies between viscometric and linear viscoelastic properties of polystyrene fluids.* PhD thesis, Massachusetts Institute of Technology. Dept. of Chemical Engineering., 1979.

[16] M. M. Cross. *Rheology of non-newtonian fluids: A new flow equation for pseudoplastic systems.* J. Colloid Sci., 20(5):417–437, 1965.

[17] H. Eyring, *Viscosity, plasticity, and diffusion as examples of absolute reaction rates.* J. Chem. Phys., 4(4):283–291, 1936.

[18] F. Ree, T. Ree, H. Eyring, *Relaxation theory of transport problems in condensed systems.* Ind. Eng. Chem., 50(7):1036–1040, 1958.

[19] A. W. Sisko, *The flow of lubricating greases.* Ind. Eng. Chem., 50(12):1789–1792, 1958.

[20] W. Herschel, R. Bulkley, *Measurement of consistency as applied to rubber benzene solutions.* Proc. Am. Soc. Testing Mater., 26, 621-629 (1926)

[21] R.R. Huilgol, Z. You, *Application of the augmented Lagrangian method to steady pipe flows of Bingham, Casson and Herschel–Bulkley fluids.* J. Non-Newtonian Fluid Mech. 128 (2005) 126–143.

[22] M. D. Normand, M. Peleg, *Flow Curves of a Herschel-Bulkley Fluid* http://demonstrations.wolfram.com/FlowCurvesOfAHerschelBulkleyFluid/ Wolfram Demonstrations Project, March 7 2011

[23] S. Lovato, G. Vaz, S. Toxopeus, G. Keetels, *Code Verification exercise for 2D Poiseuille flow with non-Newtonian fluid.* Conference: NuTTS 2018At: Cortona, Italy, October (2018)

[24] E. Mitsoulis, J. Tsamopoulos, *Numerical simulations of complex yield-stress fluid flows.* Rheologica Acta, December (2016)

[25] T.C. Papanastasiou, *Flows of materials with yield.* J. Rheol., 31, 385-401 (1987)

[26] N. Nirmalkar, R. Chhabra, R. Poole, *Laminar forced convection heat transfer from a heated square cylinder in Bingham plastic medium.* International Journal of Heat and Mass Transfer. 56. 625–639. (2013) 10.1016/j.ijheatmasstransfer.2012.08.049.

[27] A. Syrakos, G. C. Georgiou, A. N. Alexandrou. *Solution of the square lid-driven cavity flow of a Bingham plastic using the finite volume method.* Journal of Non-Newtonian Fluid Mechanics 195 (2013): 19-31.

[28] H. Taibi, F. Messelmi. *Effect of yield stress on the behavior of rigid zones during the laminar flow of Herschel-Bulkley fluid.* Alexandria Engineering Journal 57.2 (2018): 1109-1115.

[29] J. Ferziger, M. Peric. *Computational Methods for Fluid Dynamics*, Springer, Berlin, 2nd edition, (1999)

[30] J. Málek, K. R. Rajagopal, M. Ruzicka. *Existence and regularity of solutions and the stability of the rest state for fluids with shear dependent viscosity.* Mathematical Models and Methods in Applied Sciences 5.06 (1995): 789-812.

[31] H. Eberlein and M. Ruzicka, *Existence of Weak Solutions for Unsteady Motions of Herschel–Bulkley Fluids.*, Journal of Mathematical Fluid Mechanics 2012.

[32] R. I. Tanner, J. F. Milthorpe (1983) *Numerical simulation of the flow of fluids with yield stress.* Num Meth Lam Turb Flow (Eds Taylor C, Johnson JA, Smith WR), Proc 3rd Int Conf, Seattle, Pineridge Press, Swansea, 680–690

[33] M. Li, L. Tang, F. Xue, R. Landers, *Numerical Simulation of Ram Extrusion Process for Ceramic Materials.*, Proceedings of Solid Freeform Symposium, Austin, TX. Vol. 35. 2011

[34] G. Stokes, *On the Effect of the Internal Friction of Fluids on the Motion of Pendulums.* Transactions of the Cambridge Philosophical Society. 9: 8–106. 1851

[35] A Salih, *Conservation equations of fluid dynamics.*, Department of Aerospace Engineering Indian Institute of Space Science and Technology, 2011

[36] K. Vajravelu, et al. *Mathematical model for a Herschel-Bulkley fluid flow in an elastic tube.* Central European Journal of Physics 9.5 (2011): 1357.

[37] T. Roubicek, *On non-Newtonian fluids with energy transfer.* J. Math. Fluid Mech., 11, 110-125 (2009)

[38] P. Thomas-Vielma, A. Cervera, B. Levenfeld, A. Varez, *Production of alumina parts by powder injection molding with a binder system based on high density polyethylene.* J. Eur. Ceram. Soc., 28, 763-771 (2008)

[39] C. Hirsch, *Numerical Computation of Internal & External Flows: Fundamentals of Numerical Discretization.* John Wiley & Sons, Inc. USA, (1988)

[40] S. Acharya, *Analysis and FEM Simulation of Flow of Fluids in Pipes: Fluid Flow COMSOL Analysis.* (2016).

[41] H. Nguyen, T. Hoang. *Numerical Simulation of Laminar Flow Through a Pipe using COMSOL Multiphysics.* International Journal of Scienti ic & Engineering Research 8.6 (2017): 2229-5518.

[42] E. Mitsoulis, Th. Zisis. *Flow of Bingham plastics in a lid-driven square cavity.* Journal of non-newtonian fluid mechanics 101.1-3 (2001): 173-180.

[43] G. Duvaut, J. L. Lions. *Inequalities in mechanics and physics*, Berlin: Spring-Verlag (1976).

[44] P. Holmlund, *Computational Fluid Dynamic simulations of pulsatile flow in stenotic vessel models.* (2014).

[45] W. GleiBle, L. Graczyk, H. Buggisch, *Rheological Investigation of Suspensions and ceramic pastes Characterization of Extrusion Properties*, KONA Powder and Particle Journal 1993

[46] Li, M., L. Tang, R.G. Landers, and M.C. Leu, *Extrusion process modeling for aqueous-based ceramic pastes-Part 2: Experimental verification.* J. Manuf. Sci. Eng., 135:051009, 1-7 (2013b)

[47] COMSOL Multiphysics® v. 5.4. www.comsol.com, COMSOL AB, Stockholm, Sweden (2018)

[48] K. J. Hammad, G. Vradis, M. V. Otugen, M. V. Otugen, *Laminar Flow of a Herschel-Bulkley Fluid Over an Axisymmetric Sudden Expansion*, September 2001

[49] M. Vaezi, G. Zhong, H. Kalami, S.Yang, *Extrusion- based 3D printing technologies for 3D scaffold engineering.* pp. 235-254, In Functional 3D Tissue Engineering Scaffolds. Woodhead Publ., (2018)

[50] E. Mitsoulis, S. S. AbdaliN, C. Markatos, N.C. Markatos, *Flow Simulation of Herschel-Bulkley Fluids Through Extrusion Dies.* The Canadian Journal of Chemical Engineering 71(1):147-160, February 1993.

[51] "ANSYS FLUENT 12.0 Documentation", Ansys, Inc., Canonsburg, PA.

[52] dos Santos, D. Dall'Onder, et al. *Numerical approximations for flow of viscoplastic fluids in a lid-driven cavity.* Journal of Non-Newtonian Fluid Mechanics 166.12-13 (2011): 667-679.

[53] S. Durand, C. Dubois, P. Lafleur, V. Panchal, D. Park, P.Y. Paradis, D. Lepage, *Modeling of a Multilayered Propellant Extrusion in Concentric Cylinders.* Proceedings of the 2015 COMSOL Conference in Boston

[54] E. Solomon, Author V. Mathew, *3-D Comsol Analysis of Extruder Dies.* Proceedings of the COMSOL Conference 2009 Milan

[55] Multiphysics, C. O. M. S. O. L. *Chemical Engineering module Model Library.* COMSOL Multiphysics, Burlington, MA, USA (2007).

[56] S. Gürgen, W. Li, M.C. Kushan, *The rheology of shear thickening fluids with various ceramic particle additives.* Mater. Des., 15 (2016), pp. 312-319

[57] P.M. Gresho, R.L. Sani, *Incompressible Flow and the Finite Element Method, Volume 1, Advection-Diffusion and Isothermal Laminar Flow*, Wiley, 2000

[58] P.M. Gresho, R.L. Sani, *Incompressible Flow and the Finite Element Method, Volume 2, Isothermal Laminar Flow*, Wiley, 2000

[59] V. Girault, P.-A. Raviart, *Finite Element Methods for Navier-Stokes Equations: Theory and Algorithms* SPRINGER SERIES IN COMPUTATIONAL MATHEMATICS, Springer Verlag, 1986

[60] M.D. Gunzburger, *Finite Element Methods for Viscous Incompressible Flows: A Guide to Theory, Practice, and Algorithms*, Computer Science and Scientific Computing, Academic Press, 2012